NASA Technical Paper 3451

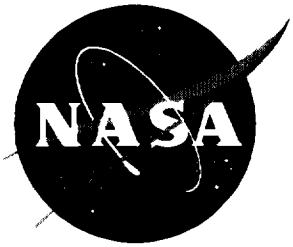

En Route Noise Levels From Propfan Test Assessment Airplane

Donald P. Garber
Lockheed Engineering & Sciences Company • Hampton, Virginia

William L. Willshire, Jr.
Langley Research Center • Hampton, Virginia

National Aeronautics and Space Administration
Langley Research Center • Hampton, Virginia 23681-0001

September 1994

The use of trademarks or names of manufacturers in this report is for accurate reporting and does not constitute an official endorsement, either expressed or implied, of such products or manufacturers by the National Aeronautics and Space Administration.

Acknowledgments

The authors would like to thank all of the people from Wyle Laboratories, Lockheed Aeronautical Systems Company, White Sands Missile Range, New Mexico State University, FAA, and the NASA Lewis and Langley Research Centers who helped acquire the experimental data for this paper. We would also like to thank those people from Langley Research Center and Lockheed Engineering & Sciences Company who assisted with theoretical calculations of propfan source noise levels. Without their talent and efforts, our research objectives would not have been accomplished.

This publication is available from the following sources:

NASA Center for AeroSpace Information
800 Elkridge Landing Road
Linthicum Heights, MD 21090-2934
(301) 621-0390

National Technical Information Service (NTIS)
5285 Port Royal Road
Springfield, VA 22161-2171
(703) 487-4650

Contents

Abstract

The en route noise test was designed to characterize propagation of propfan noise from cruise altitudes to the ground. In-flight measurements of propfan source levels and directional patterns were made by a chase plane flying in formation with the propfan test assessment (PTA) airplane. Ground noise measurements were taken during repeated flights over a distributed microphone array. The microphone array on the ground was used to provide ensemble-averaged estimates of mean flyover noise levels, establish confidence limits for those means, and measure propagation-induced noise variability. Even for identical nominal cruise conditions, peak sound levels for individual overflights varied substantially about the average, particularly when overflights were performed on different days. Large day-to-day variations in peak level measurements appeared to be caused by large day-to-day differences in propagation conditions and tended to obscure small variations arising from operating conditions. A three-dimensional ray-tracing method was used to account for atmospheric propagation of sound and predict sound levels on the ground from repeated flights performed at three representative cruise conditions. A parametric evaluation of the sensitivity of this prediction method to weather measurement and source level uncertainties was also performed. In general, predictions showed good agreement with measurements. However, the method was unable to predict short-term variability of ensemble-averaged data within individual overflights. Although variations in absorption appear to be the dominant factor in variations of peak sound levels recorded on the ground, accurate predictions of those levels require that a complete description of operational conditions be taken into account. The comprehensive and integrated methods presented in this paper have adequately predicted ground-measured sound levels. On average, peak sound levels were predicted within 3 dB for each of the three different cruise conditions.

Introduction

Historical Perspective

The Aircraft Energy Efficiency (ACEE) Program was established in 1975 to investigate methods for reducing the fuel consumption of commercial subsonic airplanes. The Advanced Turboprop (ATP) Project Office was charged with the task of developing propeller systems capable of operating at cruise Mach numbers typical of conventional turbofans with the propulsive efficiencies typical of low-speed propellers. The result of this research was a family of propellers with very thin highly swept blades called propfans. The Hamilton Standard Division of United Technologies Corporation designed, fabricated, and tested a full-scale propfan under contract as part of the Large-Scale Advanced Propeller (LAP) Program. (See ref. 1.) This full-scale propfan (designated as the SR-7L) was designed to operate at a helical tip Mach number of nearly 1.2, a flight cruise speed of Mach 0.8, and 35 000 ft above sea level.

Although the design of the SR-7L was a compromise of acoustic as well as aerodynamic and structural factors, the high-Mach-number tip generates a high noise level in the near-field with a periodic impulsive pressure function in the time domain that translates into a spectrum with distinct harmonics of the blade passage frequency. The relatively low-frequency tonal character of the propfan noise field in the cruise condition is fundamentally different from the relatively high-frequency shock cell or broadband jet-mixing noise field of a turbofan in cruise. In addition to cabin and airport community noise issues, these distinct tones, particularly at the lower harmonics, could propagate to the ground at sufficient sound levels to cause annoyance during the cruise portion of flight.

In the past, primary concern about aircraft community noise has been focused in the immediate vicinity of airports. Locally high noise levels occur on the ground during aircraft takeoff when maximum

power is used and during landing when the low approach (glide slope of 3°) at low speed exposes a large area to aircraft noise for a relatively long time period. The broadband nature of jet noise causes little noticeable effect on the ground in densely populated areas during high-altitude cruise (largest segment of a commercial flight profile) while the aircraft is en route to its destination. In less densely populated areas, particularly in parks and wilderness areas with very low-background noise levels, en route noise is audible but the broadband nature and the attenuation of high-frequency components of the shock cell noise tend to minimize annoyance. The aircraft community noise Code of Federal Regulations (CFR) (FAR Part 36 (ref. 2)), as currently enacted, requires noise measurements at only four locations all within four miles of the runway and for only takeoff and landing situations.

The propfan test assessment (PTA) airplane was developed by Lockheed Aeronautical Systems Company under a NASA contract to evaluate propfan structural integrity, propfan source noise, cabin noise and vibration, community noise related to CFR (FAR Part 36), and ground noise during en route cruise. During flights of the PTA airplane in Alabama in October 1987, the noise on the ground was audible under high-altitude cruise conditions and approached *A*-weighted levels of 60 dBA. Under similar conditions in Virginia in June 1988, the noise measured on the ground from overflights of a variety of commercial turbofan airplanes barely exceeded 45 dBA. In addition to the relatively high noise levels observed in the Alabama test, fluctuations of up to 20 dBA within periods of less than 3 sec were observed near the ground even though the propfan source level remained relatively constant. (See ref. 3.)

En Route Noise Test

Overview. The en route noise test was designed to study the propagation of propfan noise from cruise altitudes to the ground and to assess the annoyance caused by that noise. The test was conducted at the White Sands Missile Range (WSMR) where background noise was low and considerable range support was available for tracking the airplane and taking weather measurements. The test consisted of ground noise measurements taken during a series of flights over a distributed microphone array and in-flight noise measurements taken during a separate series of flights with microphones mounted on both the PTA airplane and a chase plane flying in formation. The in-flight measurements from the chase plane were included to provide reliable source levels and directional patterns that would permit an accurate estimate of propagation losses. The multiple microphones on the ground were used to estimate mean flyover noise levels, establish the confidence limits of those mean levels, and measure propagation-induced noise variability. The chase plane in-flight and the ground microphone array overflight measurements were conducted at different times to eliminate noise contamination of the ground measurements by the chase plane. The PTA airplane radar tracks and weather profile measurements were concurrently recorded to enable accurate comparison of measured results with those obtained from the propagation model.

The test was a joint effort of NASA Langley Research Center (LaRC), NASA Lewis Research Center (LeRC), and the Federal Aviation Administration (FAA). NASA LaRC coordinated the ground phase of acoustic and weather test data measurements, the FAA took independent acoustic measurements, and NASA LeRC provided and operated the PTA airplane and performed all in-flight noise measurements. Radar tracks, rawinsonde weather profiles, and communications were provided by WSMR.

Propagation study. This paper details the experimental study of long-range sound propagation from the NASA LaRC perspective: first, with a description of the experimental setup and then, a discussion of the test procedures. Experimental data analysis methods are presented next and are followed by a discussion of the experimental results. The temporal variability of sound level time histories are examined and then, the characteristics of peak sound pressure levels are established. Average peak levels, peak level variability, and data trends are discussed in turn; *A*-weighted sound pressure level data are presented.

Methods for predicting the measured sound levels during the aircraft flyovers are discussed next. The technique to combine theoretical predictions and experimental measurements into a smooth source directional estimate is presented and then coordinate transformations that are required to match the long-range propagation model are described. The long-range propagation prediction method is developed next; the basic ray-tracing method, the atmospheric model, the sound absorption model, and the technique for finding the source-to-observer ray are described. Propagation effects associated with the ray endpoints rather than the ray path are then discussed. Next, the overall prediction procedure and results are presented and the sensitivity of the method to variations in model parameters is examined.

Finally, the experimental data and predictions are compared. Variations of sound pressure level and frequency versus time are compared, nominal peak levels are compared, and prediction uncertainty is compared with measurement variability. The assessment of subjective annoyance caused by airplane en route noise has already been reported. (See ref. 4.)

Symbols

A	ray tube area
c	sound speed
d	microphone spacing
f_a	fluid frequency
f_e	emitted frequency
f_I	invariant frequency
k	scale factor
M	Mach number
$\hat{n}$	acoustic wave unit normal
p	acoustic pressure amplitude
R	propagation distance
r	source-receiver distance
$\vec{s}$	acoustic wave slowness vector
t_i	retardation time for ith microphone
$\vec{v}$	airplane velocity vector
$v_\parallel$	airplane speed along microphone array
$\vec{w}$	wind velocity vector
α	acoustic emission angle
ρ	atmospheric density
σ	standard deviation
θ	source-receiver reception angle

Subscripts:

B	boom microphone, in-flight
b	boom microphone, overflight
m	measured
p	predicted
R	source distance, in-flight
r	source distance, overflight
s	source
Θ	direction, in-flight
θ	direction, overflight

Abbreviations:

ACEE	Aircraft Energy Efficiency
AGL	above ground level
ANOPP	Aircraft Noise Prediction Program
ANSI	American National Standards Institute
ASSPIN	Advanced Subsonic and Supersonic Propeller Induced Noise program
ATP	Advanced Turboprop Project Office
CFR	Code of Federal Regulations
FAA	Federal Aviation Administration
FAR	Federal Aviation Regulations
LAP	Large-Scale Advanced Propeller Program
OASPL	overall sound pressure level
PTA	propfan test assessment airplane
WSMR	White Sands Missile Range

Experiment Description

Experimental Setup

Airplane configuration. The PTA airplane shown in figure 1 was a highly modified Gulfstream Aerospace Corporation GII with a propfan driven by a turboshaft engine mounted on the left wing. (See ref. 5.) The propfan consisted of a full-scale, 9-ft-diameter, eight-bladed, Hamilton Standard SR-7L propeller. It was powered by a modified Allison Gas Turbine Division M570 engine rated at 6000 hp contained in a Lockheed-designed nacelle that permitted adjustments of the shaft angle relative to the airplane. The nacelle tilt angle was set at $-1°$ for all of the flights reported in this paper. The airplane retained both Rolls Royce Limited 511-8 Spey turbojet engines on the aft fuselage although the left engine was operated at flight idle during acoustic tests. The PTA airplane was highly instrumented with a variety of sensors for monitoring airplane operation and measuring acoustic signatures. There were 45 flush-mounted microphones in the fuselage in a two-dimensional array and 5 flush-mounted microphones in a cantilevered boom mounted on the left wing outboard of the engine. Onboard acoustic measurements used for source level estimates in this paper were acquired with a boom-mounted microphone, that was positioned in the plane of the propeller.

In-flight acoustic measurements. The experiment consisted of two major phases: in-flight measurement of propfan source noise and ground measurement of propagated cruise noise. The in-flight

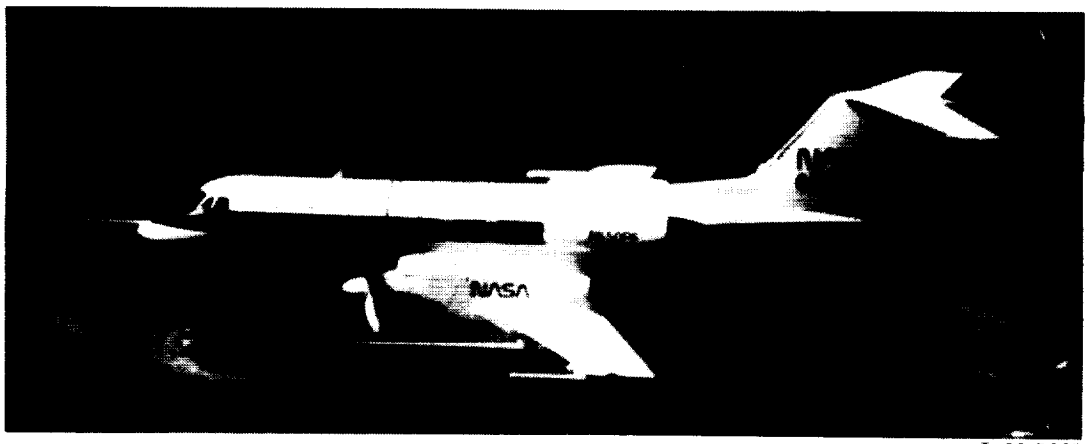

L-89-5660

Figure 1. Propfan test assessment airplane in flight.

test measurements were taken during scheduled times independent of the ground test measurements from an instrumented Gates Corporation Learjet flying in formation with the PTA airplane. The Learjet instruments measured far-field noise from the PTA airplane at specific angles while the PTA airplane onboard instruments measured near-field noise as well as a variety of airplane and engine parameters. The details of this test program have been reported by Woodward and Loeffler. (See ref. 6.) The instruments onboard the PTA airplane also measured near-field noise and a variety of airplane and engine parameters during the ground measurement phase of the test. The onboard measurement data from both phases of the test provide the basis of the far-field propfan noise estimates during the ground measurement overflights.

Weather and radar measurements. The en route noise test was performed at the White Sands Missile Range (WSMR) in New Mexico in April 1989. Background noise was low and considerable range support for radar tracking and weather measurements was available. Weather data were measured by a variety of instruments as shown in figure 2. A tethered balloon system provided continuous profile measurements of wind speed, wind direction, relative humidity, dry bulb temperature, wet bulb temperature, and pressure to 1500 ft above ground level (AGL) during each test session. Six weather stations of various heights were located in a ½-mile circle around the ground microphone array and measured temperature, wind speed, and wind direction during each session. An acoustic sounder (i.e., sodar) was located four miles to the northeast of the ground microphones and measured lower atmospheric turbulence. Finally, free-balloon rawinsonde units were released to measure wind speed, wind direction, temperature, relative humidity, and pressure up to 32 000 ft AGL before and after each session. The vertical increment of data samples was approximately 160 ft. Radar tracking of the PTA airplane was facilitated by a C-band beacon. All tracking data as well as the surveyed positions of all ground-based instruments were provided by WSMR in a common Cartesian coordinate system. Airplane position data were provided at a rate of 10 samples/sec.

Ground acoustic measurements. A diagram of the ground microphone array site is shown in figure 3. The ground microphones for this test were arrayed in a straight line at 400-ft intervals. The array was positioned on a dirt road aligned along the nominal flight path over the North Range of WSMR near the Gran Jean site. Each of the eight array elements consisted of a 42-in-square ground board with two ½-in. condenser microphones lying on their sides near the center of the board and aligned perpendicular to the nominal flight path. This configuration was designed for pressure doubling relative to free-field response for the frequencies of interest. (See ref. 7.) Each microphone face was enclosed in a foam rubber hemisphere and each microphone pair was covered with a horsehair wind screen. The horsehair wind screens were truncated cones with a base diameter of about 2 ft, a top diameter of about 1 ft, and a height of about 1 ft. Laboratory experiments indicated that the combined total acoustic absorption loss of the two wind screens was less than the estimated measurement accuracy of 0.25 dB for frequencies of less than 1000 Hz. At each array position, one microphone was connected to an analog signal conditioning system while the other was connected to a 16-bit analog-to-digital converter located in the microphone power supply. The converter sampled the analog signal from the microphone at a rate of 2344 samples/sec.

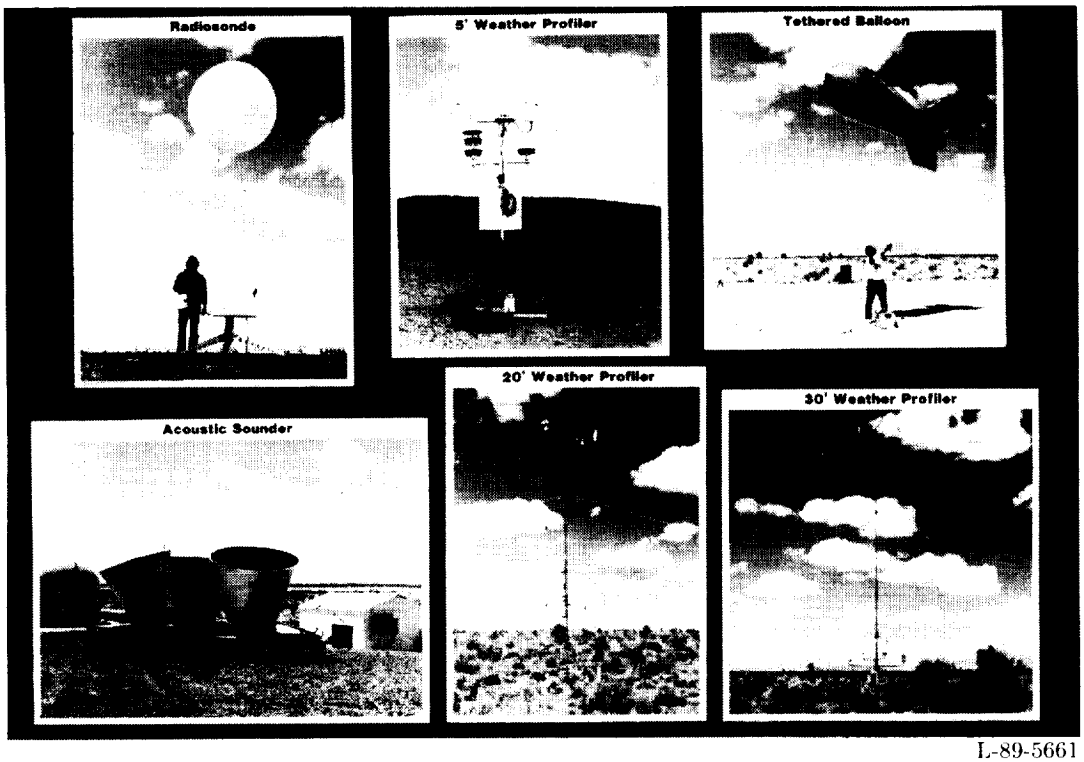

Figure 2. En route noise test weather instrumentation.

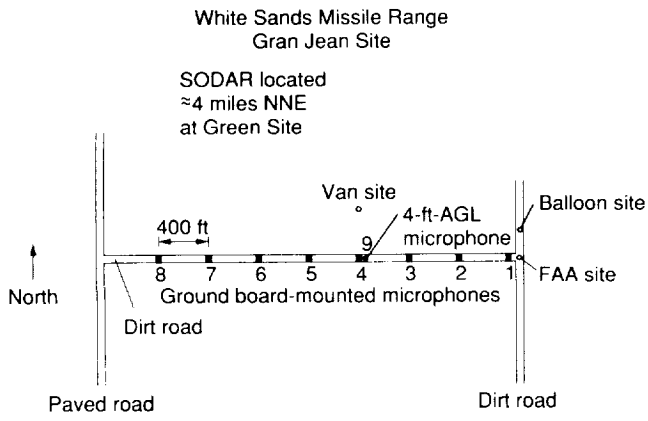

Figure 3. Diagram of ground microphone array site.

Located near one of the ground board installations were analog and digital microphones mounted 4 ft (1.2 m) above the ground. Each of the two 4-ft-AGL microphones was enclosed in a foam rubber sphere. Figure 4 is a photograph of one of the ground board installations and the adjacent 4-ft-AGL microphone. The microphones were connected by cables to instrumentation vans, which were located near the middle and about 360 ft north of the array, for signal tape recording. Two additional microphones located near the western end of the array were connected to a portable tape recorder for subjective noise studies. The FAA had a ground-mounted and a 4-ft-AGL microphone set near the eastern end of the LaRC microphone array and at a site located approximately five miles north of the array.

Figure 4. Ground board microphone installation and adjacent 4-ft-AGL microphone.

Experimental Procedure

The PTA airplane was flown to the range from El Paso, TX for each test session. Before each session, the ground array microphone systems were calibrated with pistonphone and electronic white noise

before being installed on ground boards or tripods. Five minutes of ambient noise were then recorded. All of the local weather stations were activated and a rawinsonde balloon was released. The airplane was scheduled to arrive just as the balloon cleared the test area (about an hour after its release). Radar located the airplane on the western edge of the range before the start of the first flight in each test session. The C-band radar output was displayed on a plotting board at the range control center and permitted real-time monitoring of airplane position and speed. An ideal ground track aligned with the microphone array was plotted on the board before the airplane arrived.

Ground flight controllers were in communication with the airplane crew during each test session and directed the pilot along the desired track. The airplane made a series of west-to-east and east-to-west flights over the array. Each flight was to be flown at a constant speed, altitude, and propfan rotational tip speed from the list of nominal test conditions shown in table 1. The table shows the flight altitudes above ground level; note that the ground level at the microphone array site is about 4800 ft above mean sea level. After the airplane cleared the test area at the conclusion of each session, another rawinsonde balloon was released, another 5-min ambient noise recording was made, and the microphones were rechecked with the pistonphone to measure calibration drift. Data from the digital system were then transferred to a computer workstation and briefly analyzed to verify data quality and ensure that test objectives were being met.

Table 1. Nominal Test Conditions

Flight series	Altitude, ft AGL	Mach number	Tip speed, ft/sec
100	30 000	0.7	800
200	15 000	.7	800
300	15 000	.5	800
400	9 000	.5	800
500	2 000	.5	800
600	30 000	.77	840
700	30 000	.7	700
800	30 000	.7	620

The test program was focused primarily on the flight series 100, 200, and 300 to develop a significant database which reflected a reasonable range of cruise conditions. A limited number of tests at lower altitudes, the flight series 400 and 500, were added to provide higher signal-to-noise ratio ground noise measurements for assessment of propagation model consistency. The flight series 600, 700, and 800 were included to study the effect of variations in propfan rotational tip speed on noise levels on the ground. Eighty-eight passes were flown in eight test sessions conducted on seven different days during an eleven-day period from 3 April to 13 April 1989 (two sessions on 6 April). Average actual flight conditions are summarized in table 2. Sessions were conducted at different times on these days to provide different propagation conditions. Odd numbers were assigned to west-to-east flights over the array while even numbers were assigned to east-to-west flights.

Table 2. Average Actual Test Conditions

Flight series	Altitude, ft AGL	Mach number	Tip speed, ft/sec
100	30 700	0.706	817
200	15 600	.700	820
300	15 500	.502	820
400	9 630	.501	821
500	2 360	.503	822
600	30 900	.765	831
700	31 000	.703	720
800	30 800	.704	668

Experimental Data Analysis

Radar and weather data. Radar data provided by WSMR at the conclusion of testing was in a Cartesian coordinate system referenced to a point near the microphone array and aligned with local lines of latitude and longitude. A least-squares line was fitted to the surveyed positions of the eight microphones comprising the linear ensemble-averaging array. A new coordinate system was then defined with an axis along the line of microphones. All radar data were transformed to the new coordinate system. Examination of radar data showed only one flight with significant sideline deviation from an ideal ground track over the microphone array. For the prediction procedure, the radar data were then subsampled to generate smaller data files with 0.5-sec sample spacing. Rawinsonde weather data were also transformed to the new coordinate system and atmospheric density profiles were calculated from pressure, temperature, and humidity. (See ref. 8.) The weather data from before and after each test session were then interpolated in time to provide an estimate of the local weather for each flight.

Acoustic data. All of the ground-measured acoustic data presented in this report are from the

microphone system in which an analog-to-digital converter was located in the microphone power supply. Pistonphone data were processed first to determine calibration constants. Flyover data sets were then examined for quality. Occasionally digitization faults were found and a method was devised for quickly eliminating bad data. A probability density function of the derivative of pressure was calculated for each record of acoustic data. Digitization faults showed up as extreme outliers on the density functions and were replaced with linear interpolations from adjacent valid data. The corrected data were then high-pass filtered at a cutoff frequency of 80 Hz to reduce wind noise contamination. A Chebyshev Type I low-pass filter with ripple in the pass band was used; the data were low-pass filtered in one direction, refiltered in the opposite direction to linearize phase, and then subtracted from the original data to yield a high-pass effect.

Ensemble averaging. Radar data for each flight were analyzed to determine the component of airplane velocity parallel to the microphone array. The data from each channel were then retarded by a time

$$t_i = \frac{d(i-1)}{v_{\|}}$$

for west-to-east flights or

$$t_i = \frac{d(8-i)}{v_{\|}}$$

for east-to-west flights where t_i is the retardation time for the ith microphone, d is the microphone spacing, i is the microphone number, and $v_{\|}$ is the speed of the airplane along the array. This has the effect of aligning the data records so that they form an ensemble where each element represents a statistical sample of the same random process. (See ref. 9.) After the microphone data were time-shifted, overall sound pressure level (OASPL) versus time histories were generated for each microphone by calculating a 0.5-sec mean-square pressure every 0.5 sec. Finally, the eight shifted OASPL time histories were averaged together on a pressure-squared basis to form an ensemble-averaged OASPL time history. As shown in the example in figure 5, the ensemble average exhibits less variability than the individual microphone time histories and provides a better statistical estimate of expected sound levels. Individual spectra were also averaged in the same manner with levels within each frequency band averaged on a pressure-squared basis to form an ensemble-averaged spectral time history. The averaged spectra were converted to 1/3-octave spectra, A-weighted, and integrated to create an A-weighted ensemble-averaged OASPL time history.

Ensemble statistics. The probability density function of a spectral estimate expressed in terms of squared pressure is chi-square with two degrees of freedom when only Gaussian noise is present and the product of the integration time and spectral bandwidth is equal to one. If a single tone is contained in the estimate along with Gaussian noise, the density function becomes noncentral chi-square and again has two degrees of freedom if the time-bandwidth product is one. Additionally, spectral estimates in nonoverlapping frequency bands are independent of each other. The central limit theorem states that the density function of a sum of independent random variables approaches a Gaussian function for a large number of degrees of freedom. An OASPL estimate can be written as the sum of all of the spectral estimates contained in the pressure-squared spectrum from a Fourier transform with the number of degrees of freedom given either by the number of spectral bands in the spectrum or by the product of the integration time and the spectral bandwidth. Because the integration time for individual microphone OASPL estimates was 0.5 sec and the bandwidth is given by the Nyquist frequency of 1172 Hz, the ensemble of eight OASPL estimates was assumed to be approximately Gaussian distributed. Confidence limits for a mean estimate made by averaging samples from a Gaussian distribution, such as the ensemble estimate of OASPL, can then be calculated from the sample mean and standard deviation using the t distribution.

Experimental Data

Temporal variability of ground sound levels. During flights of the PTA airplane in Alabama in October 1987, fluctuations as great as 20 dBA were measured near the ground within periods of less than 3 sec while the propfan source level remained relatively constant. (See ref. 3.) The measurements were taken with a microphone mounted 4 ft (1.2 m) above the ground. Those flight conditions approximately corresponded with the flight series 100 (30 000 ft AGL, Mach 0.7) of this test program. The OASPL time histories from each microphone of each flight in the series 100 were scanned to find the greatest fluctuation during any 3-sec period in the difference between the maximum and minimum OASPL. Examination of data from the microphone mounted 4 ft above the ground shows a maximum fluctuation of more than 18 dB. Data from the microphones mounted on ground boards have a

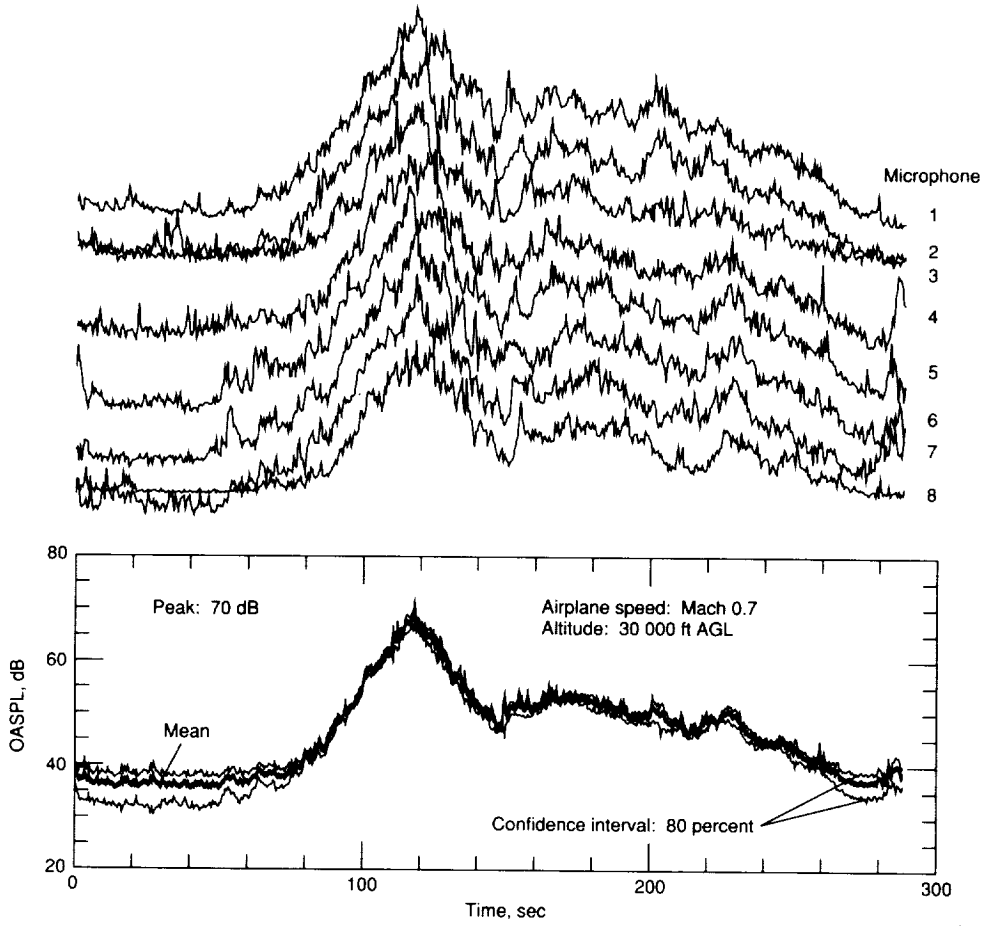

Figure 5. Example of ensemble-averaged results.

maximum fluctuation of nearly 26 dB. The ensemble averages of the eight microphones show much less variability. The greatest fluctuation in the ensemble average of any flight in series 100 is about 9 dB.

The OASPL time histories were then trend corrected to eliminate the effect of the generally increasing and then decreasing sound level from aircraft flyovers. This procedure left only fluctuations about the general shapes of the OASPL time histories. For the flight series 100, trend-corrected data from the microphone mounted 4 ft above the ground show a maximum fluctuation of less than 12 dB while trend-corrected data from the microphones mounted on ground boards have a maximum fluctuation of less than 16 dB. The greatest fluctuation in the trend-corrected ensemble average of any flight in the series 100 is about 6 dB. Trend-correction of the data indicates that the very large observed fluctuations were the result, in part, of smaller fluctuations superimposed on generally rising or falling levels. The maximum fluctuation observed among all trend-corrected OASPL time histories within each flight series are summarized in table 3 for the set of eight ground-mounted microphones, the 4-ft-AGL microphone, and the ensemble average of the eight ground microphones. The average fluctuation of OASPL is somewhat lower than these tabular values but there is still a great deal of sound level variability during relatively short time periods. Turbulence measurements were made during the flight tests to determine

Table 3. Maximum Fluctuation of Trend-Corrected Data

Flight series	Maximum OASPL fluctuation, dB, for		
	Ground microphones	4-ft-AGL microphone	Ensemble average
100	15.9	11.5	6.2
200	13.7	12.0	8.4
300	18.4	14.7	6.6
400	13.8	14.2	5.8
500	28.0	11.2	16.3
600	14.0	13.0	4.1
700	12.3	12.2	4.4
800	15.5	12.0	5.1

Table 4. Peak Ground-Measured, Ensemble-Averaged OASPL

Test session	Overflight data parameters	Overflight data for flight series, altitude (ft AGL), and Mach number of—							
		100	200	300	400	500	600	700	800
		30 000	15 000	15 000	9000	2000	30 000	30 000	30 000
		0.7	0.7	0.5	0.5	0.5	0.77	0.7	0.7
3 April	Average peak, dB	60.8	75.0	72.2					
	σ, dB	1.2	1.5	0.6					
	No. of flights	2	2	2					
4 April	Average peak, dB	69.0	72.6						
	σ, dB	0.6	0.5						
	No. of flights	4	2						
5 April	Average peak, dB	60.7	67.7	70.7					
	σ, dB	0.2	1.0	0.9					
	No. of flights	4	4	4					
6 April morning	Average peak, dB	65.1	69.7	70.2		92.4			
	σ, dB	0.8	0.8	0.2		0.7			
	No. of flights	4	4	3		2			
6 April afternoon	Average peak, dB		75.0	74.7	80.8	94.3			
	σ, dB		1.3	0.1	0.3				
	No. of flights		3	2	4	1			
7 April	Average peak, dB						68.7	65.5	65.4
	σ, dB						1.0	0.8	0.4
	No. of flights						4	4	3
8 April	Average peak, dB			74.4					
	σ, dB			0.7					
	No. of flights			11					
11 April	Average peak, dB	67.8							
	σ, dB	1.9							
	No. of flights	3							
13 April	Average peak, dB	72.2	74.3	74.3					
	σ, dB	0.8	1.4						
	No. of flights	4	4	1					
14 April	Average peak, dB						69.5	66.6	70.5
	σ, dB							0.1	1.3
	No. of flights						1	2	2
Summary	Average peak, dB	68.2	72.8	73.4	80.8	93.1	68.9	65.9	68.2
	σ, dB	2.8	2.2	1.4	0.3	1.1	0.9	0.8	2.3
	No. of flights	21	19	23	4	3	5	6	5
	Maximum, dB	73.4	76.4	75.4	81.1	94.3	70.0	66.6	71.4
	Minimum, dB	59.7	65.8	69.8	80.4	91.8	67.4	64.2	65.0

if different sound fluctuation levels correlated with different turbulence levels; however, no clear relationship between sound fluctuation and turbulence was found.

Ensemble-averaged peak ground levels. A summary of the ground-measured experimental data is shown in table 4 for each test session and flight condition. For each overflight, the maximum or peak OASPL was determined from the ensemble-averaged OASPL time history. The peak OASPL values for a particular test condition or flight series from a single test session were then averaged on a pressure-squared basis. The standard deviation σ was also determined on a pressure-squared basis; only the positive deviation was entered in the table after conversion to decibels. The number of flights included in each calculation of average OASPL and standard deviation is also shown. For each flight series, the summary data shown at the bottom of the table were also calculated on a pressure-squared basis. Eighty-six of the eighty-eight flights are represented in the table. Data from only two flights were rejected: one because the ground track showed that the sideline distance was

too great for acceptability and the other because a power failure occurred at the ground microphone site just before the airplane passed overhead.

Ensemble-averaged peak level variability. One of the most significant characteristics of the data shown in table 4 is the relatively large variation of sound pressure levels in the summary data compared with the data for individual test sessions. The standard deviation for all of the series-100 (30 000 ft AGL, Mach 0.7) data is +2.8 dB (or −10.2 dB) while the largest for any one test session of that series is +1.9 dB (or −3.5 dB) with even smaller deviations for other test sessions. The peak OASPL data for all of series 100 spanned a range of more than 13 dB while the greatest range for a single session of this series was about 4 dB on 11 April. The same pattern recurs for the other flight series. All of the flights in any one test session occurred in less than two hours on the same day. The ambient weather conditions and, hence, the acoustic propagation conditions changed very little during a single test session. However, propagation conditions changed dramatically in some cases from one day to the next. On 3 April and 5 April the average ground-measured OASPL of flight series 100 was nearly identical while average levels on 4 April were more than 8 dB higher.

Two test sessions were conducted on 6 April: one early in the morning and the other from late morning to early in the afternoon. Average sound pressure levels of flight series 200 (15 000 ft AGL, Mach 0.7) and series 300 (15 000 ft AGL, Mach 0.5) were nearly identical in the morning session. Average levels of these series were also nearly identical in the afternoon session but about 5 dB higher than in the morning session. The level for the single flight of the series 500 (2000 ft AGL, Mach 0.5) in the afternoon session exceeded the levels for both flights from that series in the morning session but by a smaller margin, probably, because of the shorter propagation path length for this series. Although the differences were small, levels from flights of the series 600, 700, and 800 (30 000 ft AGL, Mach 0.7) conducted on 14 April tended to be higher than those on 7 April.

The pattern of sound pressure levels from one test session being higher or lower than those from another session across all flight series was not consistent for the entire test matrix. Between 3 April and 13 April, average levels of flight series 100 went up dramatically, those of flight series 300 went up slightly, and those of flight series 200 went down very slightly. Also, between 5 April and the morning of 6 April, average levels of flight series 100 went up about 4 dB, those of flight series 200 went up about 2 dB, and those of flight series 300 went down less than 1 dB.

Ensemble-averaged peak level trends. As would be expected, ground sound pressure levels of the flight series 500 (2000 ft AGL, Mach 0.5) were the highest followed by those of the series 400 (9000 ft AGL, Mach 0.5) and the series 300 (15 000 ft AGL, Mach 0.5). All of these flights were at the same nominal Mach number and propeller rotational tip speed but at different altitudes. The expected levels of the flight series 200, at a nominal Mach 0.7 should have been higher than those of the series 300 at Mach 0.5 with all other flight conditions the same; however, the average of all flight series 200 was slightly lower. For some test sessions, the average ground sound levels of the flight series 200 were marginally higher but for others they were lower. There were two days in which there were flights of one series but not the other. Of particular note are the 11 flights of series 300 on 8 April for which the average level exceeded the summary average possibly because of different propagation conditions. These were the only flights conducted on that day and account for nearly half of all flights of that series. If these values are removed from the series-300 summary average, the average decreases to 72.2 dB, which is lower than the average of all of the flight series 200, and the standard deviation increases to 1.7 dB.

The average source sound pressure level of flight series 200, as recorded from the boom microphone positioned in the plane of the propeller and provided by LeRC, was 1.4 dB higher than the average source level of flight series 300. The additional difference between ground-measured levels of flight series 200 and series 300 might be due to the higher forward speed of the flight series 200. If the peak levels observed on the ground were caused by propfan sound emitted in the forward direction, then higher frequencies would be observed for flight series 200 than for flight series 300 because of greater Doppler shifting. The greater atmospheric absorption at higher frequencies would tend to reduce levels of the flight series 200 more than the series 300 and bring average ground-measured levels of the two series closer together.

The average ground sound pressure level of the flight series 600 was only slightly higher than the series 100 even though the nominal propeller rotational tip speed was 5 percent higher. Table 4 shows average actual test conditions derived from radar tracking data and PTA onboard instrumentation. The actual propfan rotational tip speed was lower than the nominal value for the flight series 600 but was higher than the nominal value for all other flight

series. Examination of data from the boom microphone reveals that the slightly higher propeller rotational tip speed of the series 600 did not significantly increase the propfan source noise levels. The average ground level of the series 700 was lower than the series 600 because the lower tip speed reduced the propfan source noise levels.

Counter to what might be expected from the operating conditions, the average ground sound pressure level of the flight series 800 was higher than the series 700 and nearly as high as the series 600. A possible explanation is that propeller helical tip speed and propeller power are more important in determination of source noise than propeller rotational tip speed. Because the forward speed of the flight series 800 was the same as the forward speed of the series 700, the helical tip speed was reduced by a smaller proportion than rotational tip speed. At the same time, the propfan blade angle of attack was increased to maintain thrust which increased the power. Boom microphone levels indicate that the source sound level remained about the same while the blade passage frequency decreased. The reduced source frequency in turn reduced atmospheric absorption; as a result, measured ground sound levels of the flight series 800 were higher than the series 700.

Ensemble-averaged peak A-weighted ground levels. A summary of A-weighted ground-measured experimental data is shown in table 5 for each test session and flight condition. For each overflight, the maximum or peak A-weighted OASPL was determined from the A-weighted, ensemble-averaged OASPL time history. The peak values for a particular test condition or flight series from a single test session were then averaged on a pressure-squared basis. The standard deviation σ was also determined on a pressure-squared basis but only the positive deviation was entered in the table after conversion to decibels. The average peak level of 61.1 dBA for the flight series 100 is in good agreement with previous tests of the PTA airplane in Alabama in October 1987 where the peak level approached 60 dBA for similar flight conditions. (See ref. 3.)

Patterns of peak sound pressure level variability are very similar to the unweighted data but trends in peak levels are slightly shifted by the weighting method. The A-weighting correction function peaks in the 2500-Hz, 1/3-octave band and decreases for lower frequencies. (See ref. 10.) The predominant component of propfan noise on the ground is the energy in the Doppler-shifted first harmonic of the blade passage frequency. If the frequency of the first harmonic is lowered, either by a decrease in the Doppler shift or a reduction in the blade passage frequency, the A-weighted level is reduced. The average A-weighted level for the flight series 200 is 6.8 dB lower than the unweighted level; the average A-weighted level for the series 300 is 8.0 dB lower than the unweighted level. Similarly, the average A-weighted level for the series 600 is 7.4 dB lower than the unweighted level; the average A-weighted level for the series 800 is 8.4 dB lower than the unweighted level.

Prediction Methods

Source Modeling

Directional pattern. An accurate map of the propfan source noise directional pattern is necessary for prediction of a ground OASPL time history. In-flight measurements of source noise were made at a variety of azimuthal and elevation angles during the en route noise test. (See ref. 6.) An interpolation method was required to give more finely spaced estimates of source sound level as a function of emission angle so that ground sound level predictions could be made for reception times that did not correspond to in-flight-measured emission angles. In preliminary analyses of these data (refs. 11–13), the NASA Aircraft Noise Prediction Program (ANOPP) was used to make source directional predictions that were then adjusted to correspond to in-flight-measured levels. For this paper, the Advanced Subsonic and Supersonic Propeller Induced Noise (ASSPIN) program (ref. 14), which is based on the method of Dunn and Farassat (ref. 15), was used to predict the source directivity for representative flight conditions of each of the flight series 100, 200, and 300. Level predictions were made for the first, second, and third blade passage harmonics at 25 elevation angles from an azimuth of 0° directly beneath the airplane. The propfan source directional pattern was assumed to be axisymmetric over the narrow range of azimuthal angles expected to be important for flights almost directly above the ground microphone array.

Predicted level adjustment. The left-hand plot in figure 6(a) shows measured and predicted far-field sound pressure level of the fundamental blade frequency for the in-flight series 100 tests. The received angle refers to the relative elevation angle between a source (the PTA airplane) and receiver (the Learjet) that are not moving with respect to each other. The only measure of source level variability between different flights over the ground microphones was provided by the microphone mounted in the boom on the PTA airplane. A method was needed to adjust the predicted levels to

Table 5. Peak A-Weighted, Ground-Measured, Ensemble-Averaged OASPL

Test session	Overflight data parameters	Overflight data for flight series, altitude (ft AGL), and Mach number of—							
		100 30 000 0.7	200 15 000 0.7	300 15 000 0.5	400 9000 0.5	500 2000 0.5	600 30 000 0.77	700 30 000 0.7	800 30 000 0.7
3 April	Average peak, dBA	53.4	68.4	64.8					
	σ, dBA	0.5	1.5	1.4					
	No. of flights	2	2	2					
4 April	Average peak, dBA	62.1	66.1						
	σ, dBA	0.7	0.5						
	No. of flights	4	2						
5 April	Average peak, dBA	53.4	60.6	62.1					
	σ, dBA	0.2	1.3	0.8					
	No. of flights	4	4	4					
6 April morning	Average peak, dBA	57.7	63.0	61.6		86.3			
	σ, dBA	0.4	0.8	0.2		0.5			
	No. of flights	4	4	3		2			
6 April afternoon	Average peak, dBA		67.9	66.9	72.9	88.3			
	σ, dBA		1.7	1.0	0.8				
	No. of flights		3	2	4	1			
7 April	Average peak, dBA						61.0	57.9	57.5
	σ, dBA						1.7	1.2	1.3
	No. of flights						4	4	3
8 April	Average peak, dBA			66.5					
	σ, dBA			0.8					
	No. of flights			11					
11 April	Average peak, dBA	60.9							
	σ, dBA	2.1							
	No. of flights	3							
13 April	Average peak, dBA	65.1	67.6	65.8					
	σ, dBA	0.7	1.5						
	No. of flights	4	4	1					
14 April	Average peak, dBA						62.8	58.4	61.9
	σ, dBA							0.5	1.2
	No. of flights						1	2	2
Summary	Average peak, dBA	61.1	66.0	65.4	72.9	87.1	61.5	58.1	59.8
	σ, dBA	2.8	2.3	1.6	0.8	1.1	1.6	1.0	2.2
	No. of flights	21	19	23	4	3	5	6	5
	Maximum, dBA	66.0	69.8	68.1	73.9	88.3	63.4	59.6	62.8
	Minimum, dBA	53.0	57.6	61.3	71.9	85.9	59.4	56.4	56.4

provide a smooth interpolation between levels measured during the in-flight tests yet account for flight-to-flight variations in average source level measured by the microphone mounted in the boom. It was assumed that the predicted source directional pattern of each flight series would be used but that the level of the pattern would be adjusted to equal the far-field in-flight-measured value at the emission angle of the greatest OASPL. Also, the source level for each flight would be further adjusted to account for the difference between the boom microphone measurement of that flight and the boom microphone measurement of the in-flight test of that series.

These assumptions lead to a correction equation of the form

$$\mathrm{SPL}_{s,r\theta} = \mathrm{SPL}_{p,r\theta} + (\mathrm{SPL}_{m,b} - k)$$

in which $\mathrm{SPL}_{s,r\theta}$ is the adjusted level to be used as the source level estimate for a particular flight at some distance and elevation angle from the propfan,

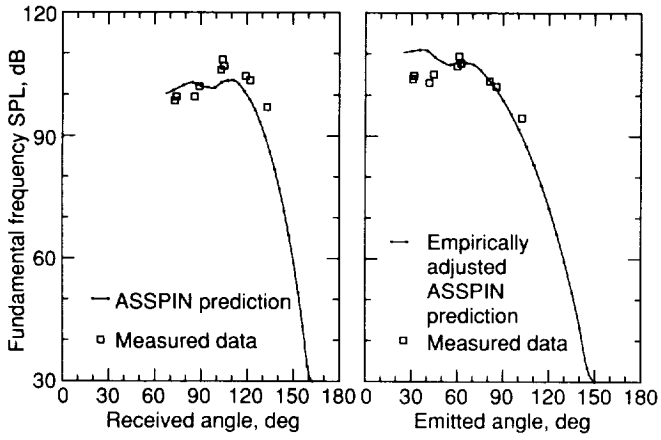

(a) Flight series 100.

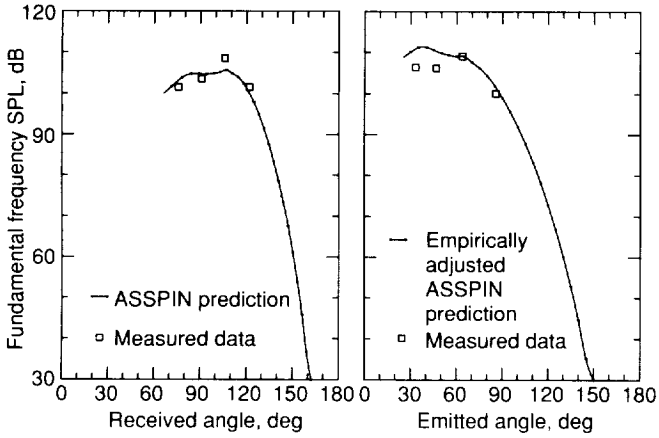

(b) Flight series 200.

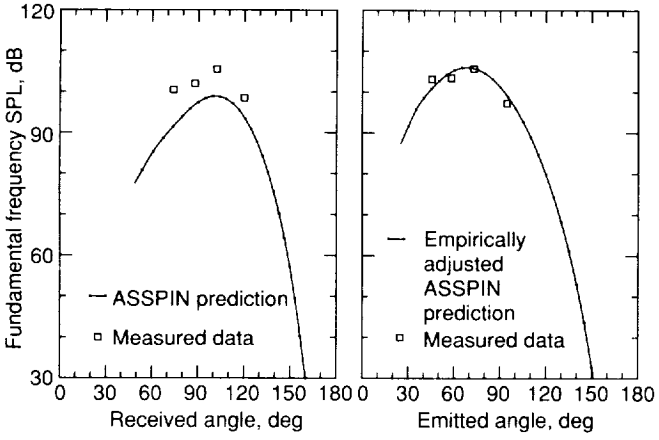

(c) Flight series 300.

Figure 6. Comparison of measured and predicted source directivity.

$\mathrm{SPL}_{p,r\theta}$ is the predicted level at a corresponding distance and elevation angle for the flight series, $\mathrm{SPL}_{m,b}$ is the average level measured at the boom microphone for that particular flight, and k is a scale factor for the flight series. The scale factor for a flight series is given by

$$k = \mathrm{SPL}_{m,B} + (\mathrm{SPL}_{p,R\Theta} - \mathrm{SPL}_{m,R\Theta})$$

in which $\mathrm{SPL}_{m,B}$ is the average level measured at the boom microphone during in-flight tests for a flight series, $\mathrm{SPL}_{m,R\Theta}$ is the level measured at a particular distance and elevation angle during in-flight tests for a flight series, and $\mathrm{SPL}_{p,R\Theta}$ is the level predicted for the corresponding distance and elevation angle for that flight series. The right-hand plot in figure 6(a) shows the measured and predicted far-field sound pressure level after adjusting the prediction. Similar plots for the series 200 and 300 appear in figures 6(b) and 6(c).

Coordinate transformation. Both predictions and measurements of in-flight source directional patterns were made in a coordinate system fixed with respect to the noise source; the source and receiver were fixed with respect to each other and the atmosphere was moving at the flight speed of the airplane. In the propagation model described below, the coordinate system is fixed with respect to an observer on the ground; the source and receiver are moving forward at the flight speed and the atmosphere in the absence of winds is stationary. The propagation model requires that the sound level as a function of emission angle (or wave normal direction) be referenced to a fixed radius from the source. The relationship between the source-receiver angle and acoustic emission angle for in-flight measurements can be seen in figure 7. The position of source and receiver at the time of emission are shown at the left; their positions at the time of reception are shown at the right. The coordinate transformation between emission and reception angles is given by

$$\cos\alpha = M\sin^2\theta + \cos\theta\sqrt{1 - M^2\sin^2\theta}$$

in which α is the wave normal (or acoustic emission) angle and θ is the angle between the source and receiver as they move in parallel during flight. Spreading loss is determined by the ratio of ray tube cross-sectional areas at the beginning and end of each ray. In the absence of refractive effects, the cross-sectional area ratio can be simply expressed as the ratio of the squares of the propagation distances. If the source sound pressure levels are to be referenced to a fixed source radius given by the distance

between the source and observer, the source levels must be adjusted to account for the propagation distance (fig. 7), which varies with the angle. The adjustment for the varying propagation distance is given by

$$\frac{R}{r} = \frac{M \cos\theta + \sqrt{1 - M^2 \sin^2\theta}}{1 - M^2}$$

in which R is the acoustic propagation distance and r is the fixed distance between source and receiver as they move together. The effect of these two transformations on the directional pattern can be seen in figure 6 where the left-hand plot is in the source-receiver coordinate system and the right-hand plot is in the ground-fixed coordinate system referenced to a fixed source radius. The directional pattern is shifted forward by the transformation so that the peak sound is emitted in the forward direction.

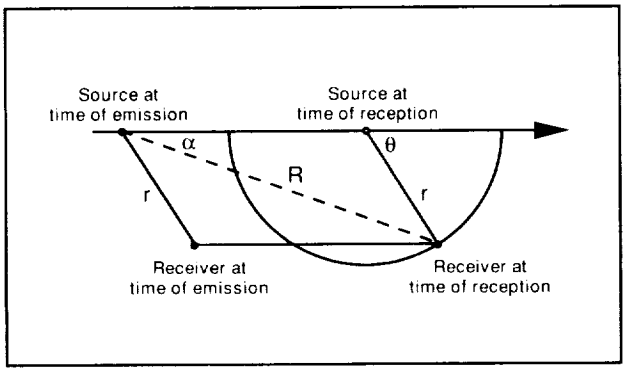

Figure 7. Transformation from reception to emission coordinates.

Propagation Modeling

Ray tracing. The choice of the propagation model depended upon the characteristics of the atmosphere and airplane as well as the goal to make temporal comparisons between measured and predicted ground noise levels. Operation of the airplane at high altitudes representative of normal cruise conditions meant that any overflight could potentially be affected by high winds moving in nearly any direction. The propfan on the PTA airplane emits highly directional periodic impulsive noise where the fundamental blade frequency has relatively short wavelengths. A comparison between measured and predicted time histories of ground noise levels directly on a synchronized time scale would be useful. Ray acoustics explicitly account for sound convection by winds, nonisotropic source directivity, and propagation time by tracing a curved line associated with a particular starting point on a wavefront. The method of using a wave slowness vector, as delineated by Pierce (ref. 16), to describe the effect of wind on a ray path also proved useful in the calculation of a fluid frequency for absorption calculations. The slowness vector is defined as the gradient of the wavefront at the location of a ray and can be written as

$$\vec{s} = \frac{\hat{n}}{c + \vec{w} \cdot \hat{n}}$$

in which $\hat{n}$ is the wave front unit normal, c is the sound speed, and $\vec{w}$ is the wind velocity vector.

Atmosphere. The atmosphere was assumed to be horizontally stratified with no vertical component of wind; both wind velocity and sound speed were assumed to be functions of altitude only. This greatly simplified integration of the ray-tracing equations. All measured atmospheric parameters as well as the calculated density were assumed to vary linearly between the altitudes at which they were measured. The square of the sound speed was determined from both temperature and humidity. Because temperature is the predominant factor in the speed of sound calculation, the square of the sound speed was assumed to vary linearly between the altitudes at which the temperature was measured.

Absorption. Derivation of the linear acoustic wave equation neglects viscous dissipative forces. This leads to a conservative equation that ignores frequency dependent losses inherent in a real atmosphere. The loss model adopted for this propagation model is based on the ANSI standard (ref. 17), but is different in some respects. The new equations proposed by Bass, Sutherland, and Zuckerwar (ref. 18) for the relaxation frequencies of oxygen and nitrogen were used in place of those appearing in the standard. The relaxation frequency equations require the saturation vapor pressure ratio. For temperatures higher than $-40°$F, the equation of Goff and Gratch was used to determine the pressure ratio. (The equation of Goff and Gratch appears in the ANSI standard document but is not part of the standard.) For temperatures lower than $-40°$F, the equation of Antoine, suggested by Sutherland (ref. 19), was used.

The work of Roy (ref. 20) was used to define a frequency invariant

$$f_I = \frac{f_e}{1 - \vec{v} \cdot \vec{s}}$$

that remains constant along a ray in which f_e is a frequency emitted by the airplane, f_I is the invariant frequency associated with that emitted frequency, $\vec{v}$ is the velocity of the airplane, and $\vec{s}$ is the wave

slowness vector. The frequency at which the sound wave excites a moving particle of air is given by

$$f_a = f_I(1 - \vec{w} \cdot \vec{s})$$

in which $\vec{w}$ is the wind velocity vector associated with that air particle. This frequency f_a is used to calculate absorption. The frequency measured by a microphone at a fixed point on the ground is just the invariant f_I. Absorption calculations require integration along the ray tube to determine the cumulative effect; however, the propagation distance used for absorption was not the same as the ray length. The propagation distance for absorption was determined from the ray path by subtracting wind convection.

Integration and convergence. The assumption of a stratified atmosphere greatly simplified integration of the ray-tracing equations by reducing them to three independent first-order differential equations: two for mutually perpendicular horizontal directions and one for time. The equations within each layer were nonlinear in the independent variable of altitude and a Gauss-Legendre numerical method was used to integrate each layer in sequence from the beginning of a ray. For each combination of source and receiver, three closely spaced rays were launched from the source at an initial estimate of the desired emission angles. Only the equations for the two horizontal directions were integrated. The varying amounts by which the rays missed the intended target were used to correct the initial launch angles by a two-dimensional secant method. The procedure was repeated until either a ray landed within 0.5 ft of the receiver, more than 100 iterations occurred without convergence, or a ray reversed direction before reaching the ground. When a ray converged on the receiver, three final rays were launched. One of the rays was integrated to determine absorption and propagation time and the other two were used to calculate ray tube area and wave front curvature at the receiver.

Blokhintsev invariant. According to Pierce (ref. 16), conservation of wave action requires that the Blokhintsev invariant

$$\frac{p^2|\vec{w} + c\hat{n}|A}{(1 - \vec{w} \cdot \vec{s})\rho c^2}$$

remain constant along an infinitesimal ray tube; by definition, p is the acoustic pressure amplitude, $\vec{w}$ is the wind velocity vector, c is the sound speed, $\hat{n}$ is the wave front unit normal, A is the ray tube area, $\vec{s}$ is the wave slowness vector, and ρ is the air density. In the absence of absorption from viscous effects, the acoustic pressure p_1 at the end of an infinitesimal ray tube can be written in terms of the acoustic pressure p_0 at the beginning and the atmospheric conditions at either end of the tube as

$$p_1^2 = p_0^2\left(\frac{A_0}{A_1}\right)\left(\frac{\rho_1 c_1}{\rho_0 c_0}\right)\left[\frac{|\vec{w}_0 + c_0\hat{n}_0|(1 - \vec{w}_1 \cdot \vec{s}_1)c_1}{|\vec{w}_1 + c_1\hat{n}_1|(1 - \vec{w}_0 \cdot \vec{s}_0)c_0}\right]$$

The first term in brackets on the right represents spreading loss if the ray tube area increases. The second term represents the familiar characteristic impedance correction. The third term is the Blokhintsev correction that is necessary to account for variations in the dynamic interaction of propagating waves with a moving medium. All three of these terms are included in received sound pressure level calculations which require only a knowledge of conditions at either end of a ray tube and involve no integration along the tube beyond what is needed to define the ray tube itself.

Ground effects. The ground is modeled as a flat surface with complex impedance. The method of Chien and Soroka (ref. 21) was used to determine the sound level above an impedance plane for an incident spherical wave. The correction for partial signal coherence suggested by Pao, Wenzel, and Oncley (ref. 22) was included and the empirical relations of Bies (ref. 23) were used to calculate the ground impedance from an estimate of the ground flow resistance. A ground flow resistance of 1000 (slug/ft^3)/sec (515 000 (kg/m^3)/sec) was assumed to be representative of the hard packed dirt road surface on which the microphones were placed. The model of Chien and Soroka assumes a straight line propagation from source to receiver on both direct and reflected paths and its equations are written in terms of path length and incident angle. Ray tracing yields curved propagation paths and wave front curvature that is not a function only of propagation distance. The Chien and Soroka equations were rewritten in terms of wave front curvature and incident angle at the location of the receiver.

Prediction

Procedure. The procedure for predicting en route noise levels on the ground was contained within a computer program developed specifically for the en route noise test. The radar, weather, and adjusted source sound pressure level data files for each flight were read. For each source position in the radar data, a search was made to find a ray that would intercept the receiver position of the first microphone of the ground array. Propagation losses were determined

Table 6. Peak Predicted Ground OASPL

Test session	Overflight data parameters	Overflight data for flight series, altitude (ft AGL), and Mach number of—							
		100 30 000 0.7	200 15 000 0.7	300 15 000 0.5	400 9000 0.5	500 2000 0.5	600 30 000 0.77	700 30 000 0.7	800 30 000 0.7
3 April	Average peak, dB	64.4	74.3	76.1					
	σ, dB	0.3	0.7	0.1					
	No. of flights	2	2	2					
4 April	Average peak, dB	66.8	75.7						
	σ, dB	0.7	0.8						
	No. of flights	4	2						
5 April	Average peak, dB	63.9	70.6	73.1					
	σ, dB	0.4	0.7	0.2					
	No. of flights	4	4	4					
6 April morning	Average peak, dB	63.2	71.4	74.5					
	σ, dB	0.4	0.6	0.2					
	No. of flights	4	4	3					
6 April afternoon	Average peak, dB		73.7	75.0					
	σ, dB		0.2	0.2					
	No. of flights		3	2					
7 April	Average peak, dB								
	σ, dB								
	No. of flights								
8 April	Average peak, dB			76.2					
	σ, dB			0.2					
	No. of flights			11					
11 April	Average peak, dB	69.2							
	σ, dB	0.6							
	No. of flights	3							
13 April	Average peak, dB	69.4	74.3	75.1					
	σ, dB	0.2	0.4						
	No. of flights	4	4	1					
14 April	Average peak, dB								
	σ, dB								
	No. of flights								
Summary	Average peak, dB	66.9	73.3	75.4					
	σ, dB	2.0	1.5	0.9					
	No. of flights	21	19	23					
	Maximum, dB	69.8	76.3	76.5					
	Minimum, dB	62.8	69.9	73.0					

for each blade passage harmonic of a ray reaching the receiver. The adjusted directional pattern of the source was interpolated to find the source level for each harmonic of the blade passage frequency at the emission angle of the ray. Propagation effects were then added to get reception levels. For each ray, the emission position, angles, and time; reception angles and time; and the propagation effects of spreading loss, characteristic impedance correction, and Blokhintsev correction were recorded. The source level, atmospheric absorption, ground effect, and reception level of each harmonic were also recorded for each ray.

Results. The predicted peak overall sound pressure levels on the ground is summarized in table 6 by test session and flight condition. All averages were calculated on a pressure-squared basis and only the positive standard deviations were entered in the table after conversion to decibels. The predicted levels include contributions of the first three harmonics of the blade passage frequency; note that the

fundamental frequency dominates. In every prediction, the single greatest propagation effect on peak level was that of spreading loss. Source levels were referenced to a distance of 1 ft so predicted spreading losses were approximately 91 dB for the flight series 100 (30 000 ft AGL, Mach 0.7) and 84 dB for both of the flight series 200 (15 000 ft AGL, Mach 0.7) and series 300 (15 000 ft AGL, Mach 0.5). Predicted atmospheric absorption of the fundamental tone averaged approximately 15 dB for flight series 100, 10 dB for flight series 200, and 8 dB for flight series 300. The ground effect added just under 6 dB for every prediction. The predicted characteristic impedance correction added nearly 5 dB for flight series 100 and just over 2 dB for flight series 200 and 300. The Blokhintsev correction was the smallest in magnitude and averaged to zero because upwind and downwind flights were generally paired.

Variations of predicted peak ground sound pressure levels between flights resulted primarily from variations in atmospheric absorption of the fundamental tone. The range of variations was about 7 dB between the largest and smallest absorption contributions to peak levels for the flight series 100, 3.5 dB for the series 200, and 2 dB for the series 300. Source level variations between flights also accounted for a significant proportion of the variation in predicted peak ground levels. The variation in the source level of the fundamental was about 4 dB for the flight series 100 and 200 and about 2 dB for the flight series 300. Variation of spreading loss between flights was only about 0.5 dB for all of the flight series. Although winds at the flight altitude approached 125 ft/sec during some flights, the Blokhintsev correction tended to contribute very little to predicted peak levels because of the steep propagation angle. However, the variation of the Blokhintsev correction between flights of the series 100 was about 0.5 dB, which is on the order of the spreading loss variation. Predicted characteristic impedance corrections and ground effects did not vary significantly between flights within any of the flight series.

Prediction Sensitivity

Source model. Predictions of noise levels on the ground depend on the validity of the source and propagation models as well as parameters used by those models. The source model accounts for the complex interaction between a finite element structural analysis code, an aerodynamics code based on an Euler equation, and an acoustics code based on the Ffowcs Williams-Hawkings equation without the quadrupole term. (See ref. 15.) The effect of small changes in model parameters on either source levels or directional patterns is not known; however, source level predictions were adjusted to match far-field values measured during the in-flight test phase and were varied in response to average boom microphone levels measured between flights during the ground measurement phase. Bias or variability in those boom microphone level measurements are directly reflected in the predicted levels at the ground. A limited number of tests were selected from the ground measurement phase to examine the temporal variability of boom microphone spectra. Spectra were calculated with the same 0.5-sec integration time that was used for analysis of ground measurements. The minimum, average, and maximum sound pressure levels of the fundamental blade passage frequency for each of the individual flights are shown in table 7.

Table 7. Boom Microphone Sound Pressure Level Variability

Flight number	Minimum SPL, dB	Average SPL, dB	Maximum SPL, dB
104	136.0	139.4	141.4
109	139.7	140.6	141.4
112	138.8	140.1	141.1
118	138.8	139.9	140.7
206	135.6	138.4	139.8
209	135.3	138.0	140.3
214	135.5	138.2	139.6
215	134.6	138.4	140.1
303	136.2	137.0	137.6
305	136.0	136.7	137.2
306	136.3	136.9	137.4
319	136.6	137.1	137.7

The greatest variability is observed in the flight series 200 with a range of levels approaching 5 dB on average. The boom sound pressure levels for the flight series 100 range over about 3 dB on average; the levels of the flight series 300 vary by only about 1 dB. Because atmospheric absorption is a strong function of frequency and plays such a significant role in determining sound levels at the ground, the temporal stability of the blade passage frequency is also of interest. The minimum, average, and maximum blade passage frequency for each of the individual flights are shown in table 8. The greatest variability is again observed in the flight series 200 with a range of frequencies approaching 5 Hz on average. The frequency range for the flight series 100 is about 2 Hz on average; the frequency of the flight series 300 varies by less than 1 Hz.

Propagation model. The propagation model uses three-dimensional ray tracing through a layered

Table 8. Boom Microphone Sound Frequency Variability

Flight number	Minimum frequency, Hz	Average frequency, Hz	Maximum frequency, Hz
104	229.4	230.8	231.5
109	230.0	230.8	231.5
112	228.8	230.1	231.3
118	229.8	230.9	231.7
206	229.1	231.0	233.2
209	229.3	231.6	234.4
214	229.8	232.6	234.9
215	229.8	232.6	234.7
303	231.5	231.9	232.1
305	231.4	231.8	232.1
306	231.4	231.8	232.1
319	231.3	231.8	232.3

atmosphere coupled with an absorption mechanism and a ground interaction model. The weather data required for calculating refraction effects, characteristic impedance corrections, Blokhintsev corrections, and absorption include temperature, humidity, pressure, density, and wind velocity. Determination of a predicted peak ground OASPL from this propagation model includes the interaction between refractive effects and absorption effects, which are complicated nonlinear functions integrated over a number of atmospheric layers. The effect of small changes in model parameters cannot be simply determined analytically. To estimate the magnitude of uncertainties in predicted levels because of uncertainties in weather and airplane parameters, a very simple bounding approach was used. Rawinsonde instrumentation reliability estimates from reference 7 were used to place upper and lower bounds on measured weather data. The ground flow resistance was arbitrarily assumed to be reliable within a factor of ten of the assumed nominal value of 1000 $(\text{slug}/\text{ft}^3)/\text{sec}$.

Parametric study. The source levels and frequencies for each flight in a flight series were assumed to vary from nominal values. The variations were equal to the average variation for the representative flights from that series and are shown in tables 7 and 8. The ray-tracing program was then run repeatedly to determine the combination of upper or lower measurement uncertainty bounds for each profile or parameter that gave the greatest increase or decrease in predicted peak OASPL. This procedure does not provide the highest peak OASPL predictions that are possible but it does give an estimate of the magnitude and source of prediction uncertainty. The greatest predicted uncertainty occurred for the flight series 200 (15 000 ft AGL, Mach 0.7) where the range of predictions (i.e., the greatest prediction minus the least prediction) for an individual flight was as low as 6 dB in one case and as high as 8 dB in another. The range of predictions for individual flights varied from 5 dB to 7 dB for the flight series 100 (30 000 ft AGL, Mach 0.7) but only from 2 dB to 4 dB for the series 300 (15 000 ft AGL, Mach 0.5).

The greatest contributor to uncertainty in predicted peak levels is the variability of source levels measured by the boom microphone. Atmospheric absorption and ground effects contribute to a lesser degree. Absorption uncertainty is caused by a combination of source frequency variability and humidity measurement inaccuracy, particularly at very high altitudes where the temperature drops below −40°F. For this reason, absorption uncertainty is roughly 2 dB for flights at 30 000 ft AGL and about 1 dB for flights at 15 000 ft AGL. The uncertainty of approximately 1 dB from the ground effect is large because the assumed range of ground flow resistance is two orders of magnitude, which reflects a lack of confidence in the nominal value assumed for this parameter. Spreading loss, the characteristic impedance correction, and the Blokhintsev correction are relatively unaffected by changes in either source or atmospheric characteristics within the ranges assumed.

Two significant factors ignored in this parametric study are the directional pattern of the source and the weather variability exclusive of measurement accuracy. The emission angles corresponding to the predicted peak ground levels fell within the range of 72° 76° for flight series 100, 67°–76° for series 200, and 75°–78° for series 300. Examination of the source level versus emission angle plots at the right of figure 6 shows that these emission angles correspond to a range of angles for which the adjusted source predictions appear to be in close agreement with the measured data. The accuracy of weather data is more difficult to assess. Rawinsondes provide weather data only for the times and positions described by a rising and drifting balloon. Local weather for each flight was estimated by interpolating data from balloon releases before and after each test session but the probable temporal and spatial limits on the variability of these data are unknown. The potential error introduced by this uncertainty probably exceeds that of instrumentation reliability.

Comparison of Data With Predictions

Temporal Evolution of Received Sound

OASPL versus time. Because a propeller airplane flies at essentially constant conditions, the

sound level at a fixed spot on the ground beneath the flight path rises to some peak level and then falls while the frequencies of the propeller tonal harmonics have Doppler shifts from above to below their unshifted values. When comparing the predicted and measured sound levels, these two features of the received sound will be considered separately. Predicted and measured OASPL time curves for six overflights are shown in figure 8. In each plot, the three relatively smooth curves are the lower bound, nominal, and upper bound predictions based on the best estimates of source, weather, and ground parameters along with their assumed errors as discussed before. The three jagged curves are the lower 80-percent confidence bound, average, and upper 80-percent confidence bound from the ensemble average of the eight ground-mounted microphones. The curves in each plot are all referenced to an arbitrary but common time scale.

The results of flight 109 are shown in figure 8(a). This flight from the series 100 (30 000 ft AGL, Mach 0.7) took place on the morning of 5 April 1989. The prediction curves are generally centered over the peak of the ensemble-averaged measurement, but the nominal prediction peak clearly exceeds even the upper 80-percent confidence bound of the measurement. However, the peak of the lower bound prediction is less than the peaks of both the upper 80-percent confidence bound and the average of the measured data. The magnitudes of these differences are fairly small and the peak of the nominal prediction exceeds that of the ensemble average by less than 3 dB. Figure 8(b) shows the results for flight 112 which took place on the following morning of 6 April. The prediction curves are again generally centered over the peak of the ensemble-averaged measurement but the nominal prediction peak is now less than that of even the lower 80-percent confidence bound of the measurement. However, the peak of the upper bound prediction is greater than the peak of the lower 80-percent confidence bound of the measured data. The magnitudes of these differences are still small and the peak of the nominal prediction is less than 3 dB below that of the ensemble average.

Results of two flights from the series 200 (15 000 ft AGL, Mach 0.7) are shown in figures 8(c) and 8(d) for flight 206 from the morning of 5 April and flight 215 from the afternoon of 6 April, respectively. As in the previous pair of plots, an example is shown for an over and for an underprediction. In both examples, the confidence bounds of the ensemble average and the estimated error bounds of the prediction overlap; the difference between the peak of the nominal prediction and the peak of the ensemble-averaged measurement is less than 2 dB. Although the prediction curves are nearly centered over the peak of the ensemble-averaged measurement, the shapes of the prediction and measurement curves for these series-200 examples do not agree as well as in the series-100 examples above. The measurement curves show a very abrupt increase in OASPL just before the peak and an equally abrupt decrease following the peak; the prediction curves show a more gradual increase and decrease. The shapes of the measurement and prediction curves for the series-100 examples above showed much better agreement.

Results of two flights from the series 300 (15 000 ft AGL, Mach 0.5) are shown in figures 8(e) and 8(f) for flight 305 from the morning of 5 April and flight 319 from the morning of 8 April, respectively. Unlike the previous plots, these are both examples of overpredictions because there were no underpredictions for any of the nominal predictions for flight series 300. The confidence bounds of the ensemble average overlap the estimated error bounds of the prediction in these two examples; this is not true for all of the flight series 300. However, the difference between the peak of the nominal prediction and the peak of the ensemble-averaged measurement is less than 4 dB in both cases. The prediction curves are also nearly centered over the peak of the ensemble-averaged measurement but the shapes of the curves for these series-300 examples show some differences. The curves agree reasonably well when the OASPL is increasing but diverge somewhat when the OASPL is decreasing.

None of the prediction curves in figure 8 exhibit the short term variability shown by the ensemble-averaged measurement curves. The levels and locations of the peaks of the prediction seem to agree fairly well on average with those of the measurements but not in detail. The only prediction parameter that varied with time was the airplane position determined by radar. Weather parameters that varied during overflight might account for the observed variability in the sound level but neither the prediction model nor the weather measurements allowed for temporal or spatial variation. A more complex prediction model that includes source level and frequency variability coupled with some stochastic atmospheric variability might yield the same general characteristics of the measured sound curves but exact predictions are impossible.

Frequency versus time. Although the prediction curve peaks appear to be nearly centered over the peaks of the ensemble-averaged measurement curves, agreement is not perfect. Possible causes

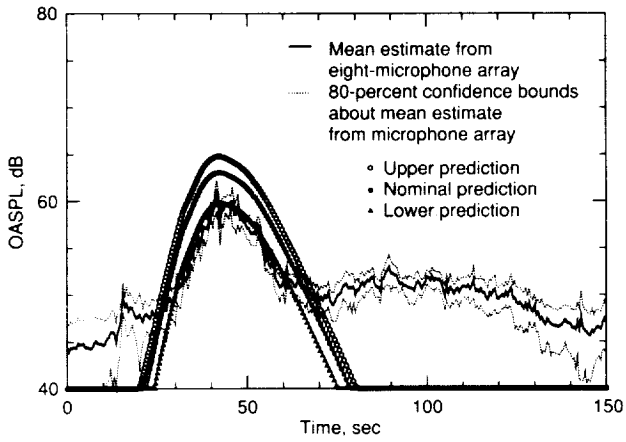

(a) Flight 109.

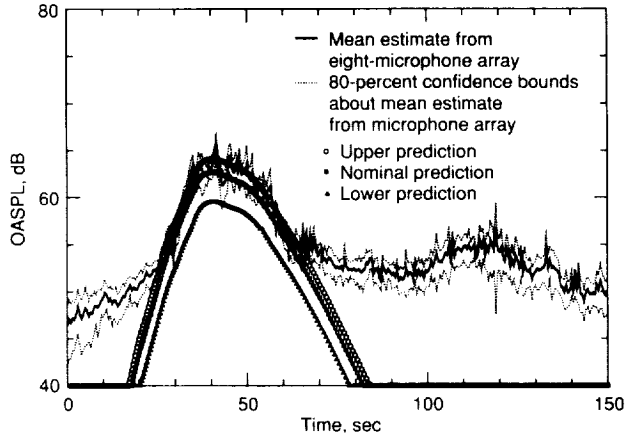

(b) Flight 112.

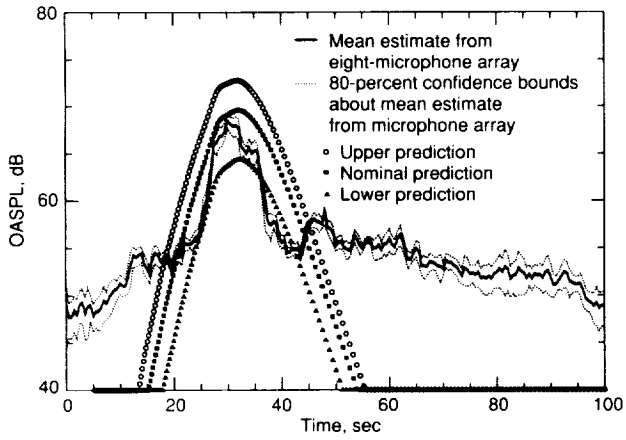

(c) Flight 206.

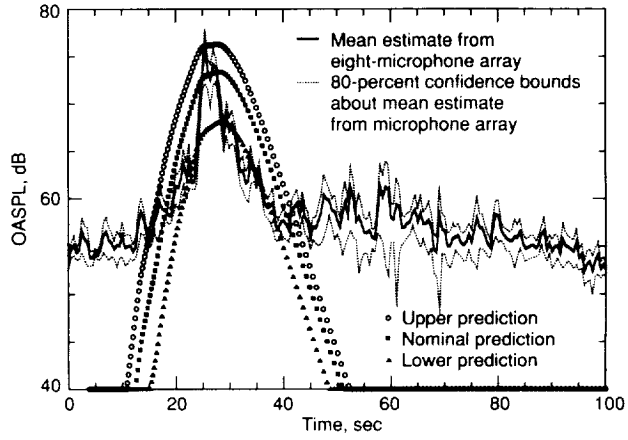

(d) Flight 215.

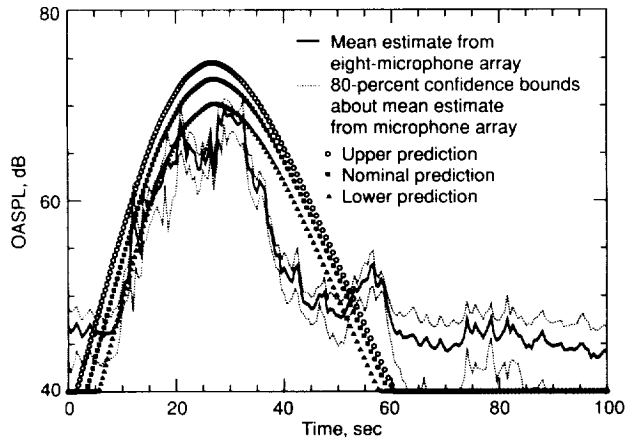

(e) Flight 305.

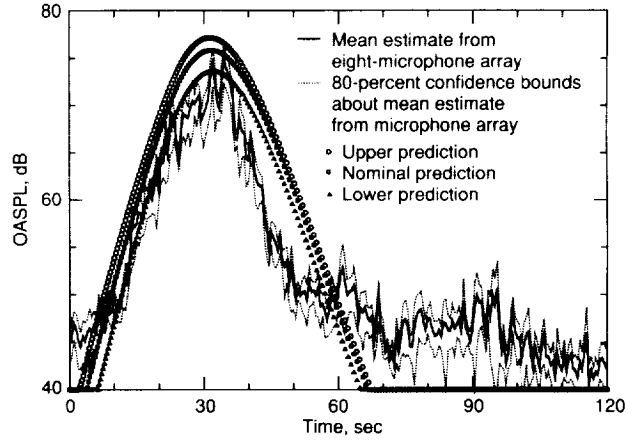

(f) Flight 319.

Figure 8. Comparison of ground-measured and predicted OASPL.

of the disagreement include inaccurate source directional estimates, propagation effects, poor time synchronization between prediction and measurement, and/or Doppler errors from inaccurate ray paths. Comparison of the spectral content of the measured sound with predicted locations of the tones indicates that time synchronization and Doppler shift were treated correctly. Contour plots of ground-measured spectra compared with predicted propfan harmonics are shown in figure 9. In each plot, the smooth curves are the predicted received frequency of the fundamental blade passage frequency, harmonics, and subharmonics calculated for an eight-bladed propeller. The gray scale shading is a flooded contour plot of the measured spectrum as it evolves over time with the darker shading corresponding to higher spectral sound levels. The curves and contours in each plot are all referenced to a common time scale based on the radar-measured time overhead.

The results of flight 109 are shown in figure 9(a). This plot corresponds to that shown in figure 8(a). The plot of the predicted fundamental tone clearly overlays a region of dark shading that corresponds to a measured tone with a time-varying Doppler shift. More difficult to discern is another region of shading that corresponds to twice the fundamental frequency and agrees very nicely with the predicted reception of the second harmonic. The sound level of the second harmonic is much lower than that of the fundamental frequency and contributes very little to the overall sound pressure level. Preferential absorption of higher frequencies by the atmosphere substantially reduces the sound levels of blade passage frequency harmonics measured from long range when compared with short range. Tones corresponding to the third and fourth subharmonics (S3 and S4) of the blade passage frequency are very difficult to discern. These tones can be seen with a very high resolution plot on a computer workstation screen but do not reproduce very well on paper. The tones appear during a time span from approximately overhead to 15 sec later and correspond to a range of emission angles slightly forward of overhead.

The results of flight 206 are shown in figure 9(b). This plot corresponds to that shown in figure 8(c). The plots of the predicted fundamental and second harmonic tones clearly overlay regions of dark shading that correspond to measured tones with time-varying Doppler shifts. Although more difficult to see, another region of shading is still visible that corresponds to three times the fundamental frequency and agrees very nicely with the predicted reception of the third harmonic. Again, the sound levels of the second and third harmonics are much lower than that

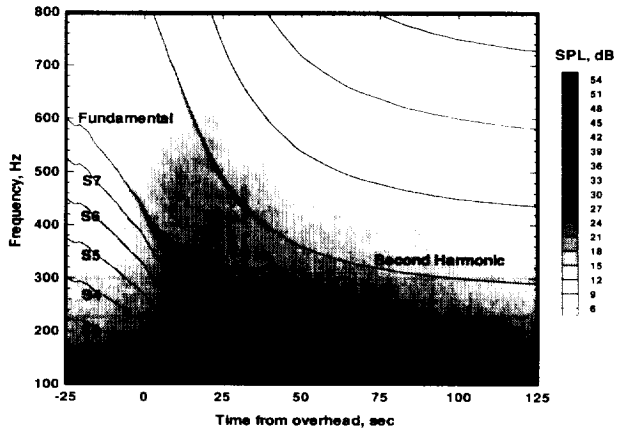

(a) Flight 109.

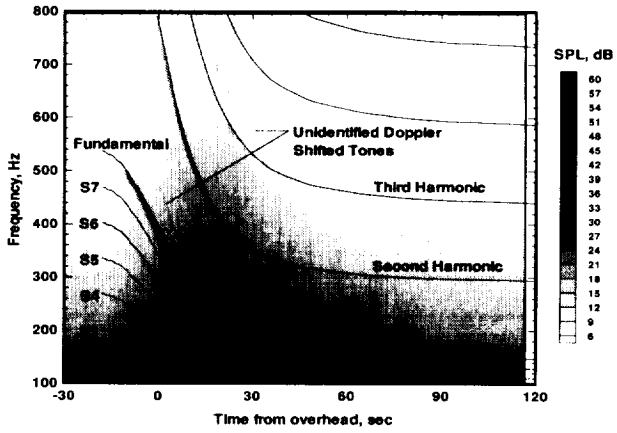

(b) Flight 206.

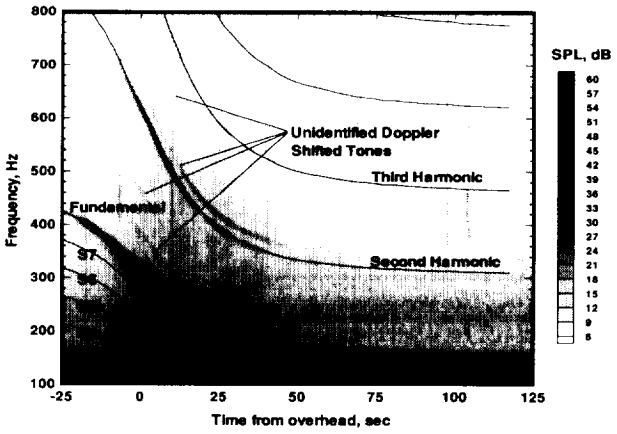

(c) Flight 305.

Figure 9. Comparison of spectral content of ground-measured and predicted sound.

of the fundamental and contribute very little to the overall sound pressure level. Also, as in the previous plot, tones are plotted which correspond to the third and fourth subharmonics (S3 and S4) as well as the fifth and sixth subharmonics (S5 and S6) of the blade passage frequency. They also appear during a time span that corresponds to a range of emission angles slightly forward of overhead. In addition to tones that clearly correspond to the propfan source, two other tones were measured that had a time-varying Doppler shift similar to the propfan. These tones obviously must be associated with the PTA airplane but cannot be directly linked with the propeller.

The results of flight 305 are shown in figure 9(c). This plot corresponds to that shown in figure 8(e). The plots of the predicted fundamental and second harmonic tones clearly overlay regions of dark shading that correspond to measured tones with time-varying Doppler shifts. Another faint region of shading corresponds to three times the fundamental frequency and agrees very nicely with the predicted reception of the third harmonic. Again, the sound levels of the second and third harmonics are much lower than that of the fundamental and contribute very little to the overall sound pressure level. Also, tones corresponding to the third, fourth, fifth, and sixth subharmonics (S3, S4, S5, and S6) of the blade passage frequency are visible. They appear during a time span that corresponds to a range of emission angles slightly forward of overhead. In addition to tones that clearly correspond to the propfan source, there are four tones with a Doppler shift that varies in time similar to the propfan. These tones obviously must be associated with the PTA airplane but cannot be directly linked with the propeller.

Given the excellent agreement between the measured tones and their predicted location, any differences between the positions of predicted and measured sound level peaks can be assumed to result from inexact source directional estimates or imperfectly modeled propagation effects rather than incorrectly synchronized predictions. The subharmonics that are present in ground-measured spectra but absent from in-flight-measured spectra suggest either a propagation-induced or a direction dependent noise source that appears below the propfan but not to the side at the boom microphone location and may be caused by nonaxial inflow.

Peak Sound Level

Comparison of nominal peak levels. The examples presented above indicate that the methods for predicting the characteristics of sound levels and tonal frequencies on the ground over time are reasonably accurate. The examples show both over and underpredictions of the peak sound levels measured during overflights. Comparisons between the measured and predicted peak OASPL on the ground for all of the individual overflights in each of the three en route flight conditions are shown in figure 10. The peak value of the ensemble-averaged OASPL for every overflight of each series is plotted against the corresponding peak of the nominal prediction. A symbol falling on the dashed diagonal line would indicate exact agreement between the measured and predicted peak sound level while a symbol to the right (or under) would indicate overprediction. Also, each plot includes a linear regression curve of the measured levels on the predicted levels showing the general trend of agreement. The 80-percent confidence bounds around the regression curve provide a measure of confidence on that general trend.

The results of the flight series 100 (30 000 ft AGL, Mach 0.7) are shown in figure 10(a). There is no exact agreement between the predicted and measured peaks; however, the regression line shows that there is a general trend of higher predictions corresponding to higher measurements. The range of measured peaks is slightly greater than the range of predicted peaks and that is reflected in the regression line having a slope greater than one. The dashed diagonal line representing perfect prediction lies just outside the 80-percent confidence bounds around the regression curve. The average of all of the peak predictions is about 0.5 dB lower than the average of all of the peak measurements. The greatest overprediction is less than 4 dB and the greatest underprediction is less than 5 dB.

The results of the flight series 200 (15 000 ft AGL, Mach 0.7) are shown in figure 10(b). A couple of cases show nearly perfect agreement between the predicted and measured peaks and the regression line shows the same general trend of higher predictions corresponding to higher measurements seen in the previous plot. The range of measured peaks is slightly greater than the range of predicted peaks and that is again reflected in the regression line having a slope greater than one. The dashed diagonal line representing perfect prediction lies farther outside the 80-percent confidence bounds than in the previous plot. For this flight series, the average of all of the peak predictions is about 1 dB higher than the average of all of the peak measurements. The greatest overprediction is less than 4 dB and the greatest underprediction is less than 3 dB.

The results of the flight series 300 (15 000 ft AGL, Mach 0.5) are shown in figure 10(c). In every case,

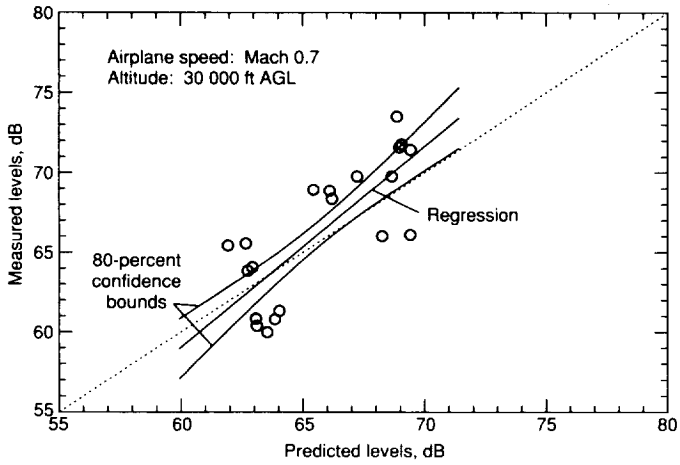

(a) Flight series 100.

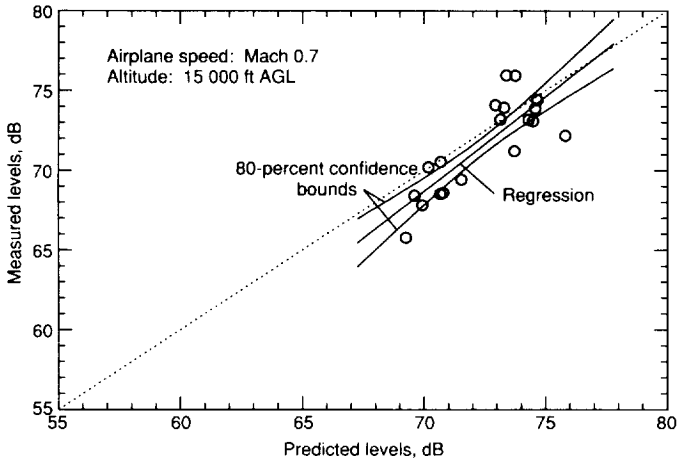

(b) Flight series 200.

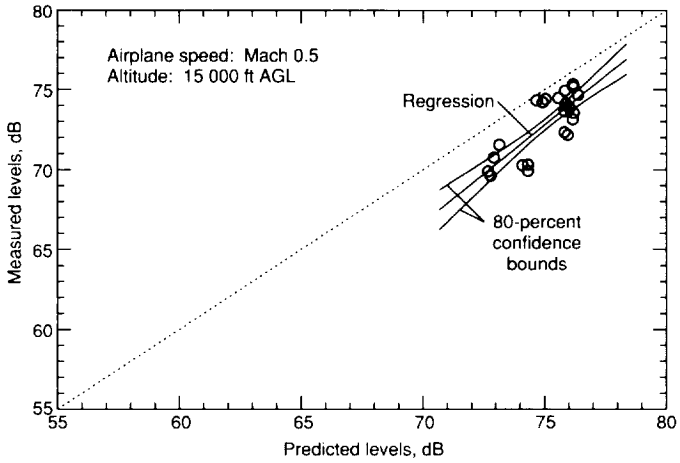

(c) Flight series 300.

Figure 10. Measured and predicted peak OASPL and regression fit.

the predicted peak exceeds the measured peak. The regression line, though, shows the same general trend of higher predictions corresponding to higher measurements seen in the previous plots. The range of measured peaks is slightly greater than the range of predicted peaks and that is again reflected in the regression line having a slope greater than one. The dashed diagonal line representing perfect prediction lies well outside the 80-percent confidence bounds. For this flight series, the average of all of the peak predictions is just over 2 dB higher than the average of all of the peak measurements. The greatest overprediction is just over 4 dB and the least overprediction is less than 0.5 dB.

Comparison of peak level bounds. The plots in figure 10 show a comparison between the peak of the ensemble average of eight microphones and the peak of the nominal prediction for each flight in the series 100, 200, and 300. However, as discussed before, there is some uncertainty in an ensemble-averaged estimate; that uncertainty can be quantified by a confidence interval. There is also some uncertainty in the prediction because of the uncertainty associated with the input parameters on which the prediction is based. That uncertainty is quantified in this paper by an upper and lower bound based on estimates of the possible uncertainty of the input parameters. The relative effect of both types of uncertainty is shown in figure 11. The peak value of the ensemble-averaged OASPL for every overflight of each series is plotted against the corresponding peak of the nominal prediction, as in the previous figure. A box is drawn around each symbol representing an overflight. The vertical extent of each box is defined by the peaks of the upper and lower 80-percent confidence bounds of the eight-microphone ensemble. The horizontal extent of each box is defined by the peaks of the upper and lower bound predictions.

The results of the flight series 100 (30 000 ft AGL, Mach 0.7) are shown in figure 11(a). The dashed diagonal line representing perfect prediction intersects every box except that of flight 113 where the lower 80-percent confidence bound peak exceeds the upper prediction bound peak by less than 1 dB. The results of the flight series 200 (15 000 ft AGL, Mach 0.7) are shown in figure 11(b). In this plot, every box overlaps the line of perfect prediction. The results of the flight series 300 (15 000 ft AGL, Mach 0.5) are shown in figure 11(c). The majority of the boxes overlap the line of perfect prediction; four of them do not. The range of the measurement confidence bounds varies from flight to flight but tends to average fairly consistently across flight

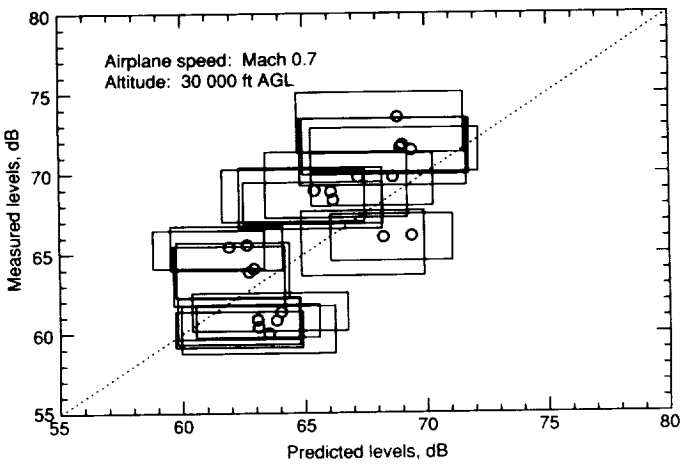

(a) Flight series 100.

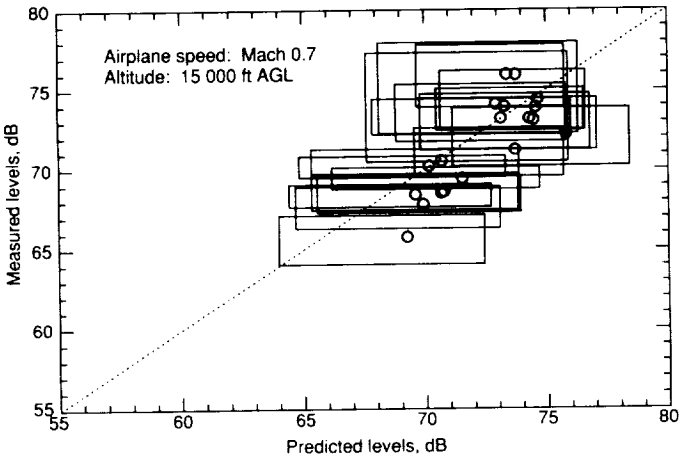

(b) Flight series 200.

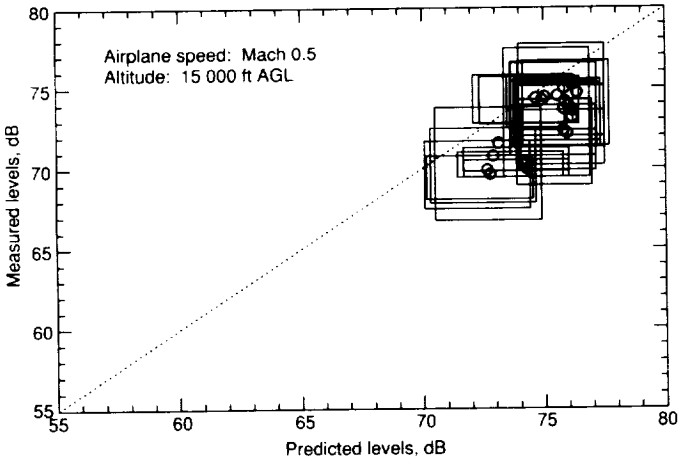

(c) Flight series 300.

Figure 11. Measured and predicted peak level comparisons and estimated error bounds.

series. The average range of the measurement confidence bounds is about 3 dB for both the flight series 100 and 200 and about 4 dB for the flight series 300. However, the range of the prediction bounds varies across the different flight series. The average range of the prediction bounds is about 6 dB for the flight series 100, 8 dB for the series 200, and 4 dB for the series 300.

For the flight series 300, the relatively small range of prediction bounds and the relatively large average overprediction are an indication that the prediction error may be systematic rather than random for that series. Review of the test procedure gives clues as to the possible source of the apparent systematic error. Several overflights from each of the flight series 100, 200, and 300 were performed during many of the test sessions. Each flight from a test session was analyzed with weather and radar data from a common source with an identical propagation model. The only feature of the prediction that was unique for the series 300 was the source level directional pattern.

There are several possible sources of systematic error. The first is that the in-flight experimentally measured source levels for the flight series 300 are too high. This seems unlikely because the levels for that flight series are very close to those of the other flight series where the signal-to-noise ratio is high. Another possibility is that the actual source directivity is sensitive to small changes in the inflow angle. A comparison of the angle-of-attack measurements for in-flight tests and en route overflights does not show a systematic difference that would cause different directional patterns. A third possibility is that the predicted directional pattern is in error. However, the estimated source emission angles corresponding to the peak ground levels are very close to the angle of the measured source strength to which the predicted directional pattern was adjusted. No single unambiguous cause for the systematic error seems to exist. In relative terms, the average error of 2 dB is small.

Summary of Results and Conclusions

The en route noise test was designed to study the propagation of propfan noise from cruise altitudes to the ground and to assess the annoyance caused by that noise. It was conducted at the White Sands Missile Range (WSMR). The ground noise phase of the test consisted of ground noise measurements made during repeated flights over a distributed microphone array. In-flight measurements of propfan source levels and directional patterns were made by a chase plane flying in formation with the PTA airplane during the in-flight phase of the test. Radar tracks

of the PTA airplane and weather profile measurements were concurrently recorded during the ground noise phase to ensure accurate propagation modeling. Multiple microphones in a linear array on the ground were used to provide ensemble-averaged estimates of mean flyover noise levels, establish confidence limits for those means, and measure propagation-induced noise variability. A total of 88 overflights were completed at various altitudes and speeds.

The acoustic data were analyzed by removal of low-frequency wind noise with a digital filter and then conversion of the pressure time histories to OASPL and spectral time histories with a 0.5-sec averaging time. Individual microphone results were ensemble-averaged and peak levels of the resulting average OASPL time histories were examined. Peak levels for different flights from within each flight series varied substantially about the average, particularly for the series 100, 200, and 300 in which overflights were performed on many different days. The range of peak levels within a particular test session tended to be smaller than the range of peak levels for the entire flight series. The large day-to-day variations in peak level measurements appeared to be caused by large day-to-day differences in propagation conditions. Propagation conditions within a particular test session appeared to change very little and the peak levels showed correspondingly less variability.

The large variations caused by day-to-day propagation differences tend to obscure small variations arising from operating conditions. Careful examination of data tends to reveal consistent trends but also what appear to be anomalies. As expected, the flight series 200 (15 000 ft AGL, Mach 0.7) caused higher peak sound levels at the ground than the series 100 (30 000 ft AGL, Mach 0.7) because of the shorter propagation path. Similarly, the flight series 300 (15 000 ft AGL, Mach 0.5), series 400 (9000 ft AGL, Mach 0.5) and series 500 (2000 ft AGL, Mach 0.5) caused progressively higher peak sound levels on the ground. Although the peak levels from the flight series 200 (15 000 ft AGL, Mach 0.7) overlap those from the series 300 (15 000 ft AGL, Mach 0.5) the slower flight series 300 tends to have a generally higher level at the ground despite the lower source level measured by the boom-mounted microphones. Also, the flight series 800 (30 000 ft AGL, Mach 0.7) with a relatively low propeller rotational tip speed exhibited a higher peak sound level on the ground than did the flight series 700 (30 000 ft AGL, Mach 0.7) which had a higher rotational speed.

A three-dimensional ray-tracing method was used to account for atmospheric propagation of sound and predict sound levels on the ground from the flight series 100, 200, and 300. The method of Dunn and Farassat (ref. 15) was used to calculate the propfan source directional pattern; in-flight measurements of the source (ref. 6) as well as boom microphone measurements were used to adjust the level of the directional patterns. The source-receiver coordinates were transformed to emission coordinates and then refraction, spreading, absorption, characteristic impedance, Blokhintsev, and ground effects were predicted by the propagation program. In general, the nominal predictions agreed fairly well with the measurements. The shapes of individual OASPL time history predictions agreed fairly well with the ensemble-averaged experimental data curves. Plots of spectra versus time showed excellent agreement between predicted and measured propfan tone frequencies.

Despite the good agreement between predicted and measured data, the following observations are noted:

1. Source and propagation modeling explains some of the variation in average peak level results but is unable to account for short-term variability of ensemble-averaged data from individual runs or the more extreme variations between microphones. The limited turbulence measurements recorded in the test program show no clear correlation with the observed short-term sound level variability.

2. Absorption plays a substantial role in determining the peak sound levels on the ground. Although the absorption model used here is not considered to be valid for the very low temperatures occurring over most of the propagation path, the predictions on the average agreed surprisingly well with measurements. Any correction of measured sound data to standard atmospheric conditions or to a nominal flight configuration when performing high-altitude overflights is subject to question because of the inability to accurately measure the characteristics of the entire propagation path and the inherently greater inaccuracy of long-range propagation modeling compared with short-range modeling.

3. Estimation of sound levels on the ground from propfan airplanes operating under cruise conditions must account for a complete operational scenario. The change of a single operational parameter can have unforeseen consequences because of the complex interactions of all the variables which determine the sound level received on the ground. For example, a reduction of the rotational speed of the propeller may reduce the maximum source

noise level but it may also change the angle at which the peak sound is emitted, reduce the source frequency, and change the pitch attitude and speed of the airplane in flight. The sound level on the ground may then be higher or lower depending on the precise interaction of all of these effects. The lower airplane speed and reduced frequency also result in less attenuation from atmospheric absorption. The direction and magnitude of changes in attitude and peak sound direction may either increase or decrease the sound level.

The comprehensive and integrated methods presented in this paper appear to have adequately predicted ground-measured sound levels. On average, peak sound levels were predicted with less than 3 dB error for the three flight series 100, 200, and 300. Prediction errors for peak sound levels of individual flights were nearly 5 dB in some cases. However, within each flight series, the higher measured peaks generally corresponded with higher predicted peaks and vice versa. Plots showing confidence bounds on ensemble-averaged experimental data as well as estimates of prediction uncertainty indicated that nominal prediction errors were quite small.

NASA Langley Research Center
Hampton, VA 23681-0001
June 10, 1994

References

1. DeGeorge, C. L.: *Large-Scale Advanced Prop-Fan (LAP) Technology Assessment Report.* NASA CR-182142, 1988.

2. Code of Federal Regulations. Title 14, Part 36—Noise Standards: Aircraft Type and Airworthiness Certification, Jan. 1990.

3. Rickley, E. J.: En Route Noise: NASA Propfan Test Aircraft (Calculated Source Noise). *FAA/NASA En Route Noise Symposium*, Clemans A. Powell, comp., NASA CP-3067, 1990, pp. 41 59.

4. McCurdy, David A.: *Annoyance Caused by Aircraft En Route Noise.* NASA TP-3165, 1992.

5. Little, B. H.; Poland, D. T.; Bartel, H. W.; Withers, C. C.; and Brown, P. C.: *Propfan Test Assessment (PTA)—Final Report.* NASA CR-185138, 1989.

6. Woodward, Richard P.; and Loeffler, Irvin J.: Inflight Source Noise of an Advanced Full-Scale Single-Rotation Propeller. AIAA-91-0594, Jan. 1991.

7. Willshire, William L., Jr.; and Nystrom, Paul A.: *Investigation of Effects of Microphone Position and Orientation on Near-Ground Noise Measurements.* NASA TP-2004, 1982.

8. Hoidale, Marjorie M.; Dayton, Michael P.; and Newman, Lamar: *Atmospheric Structure. Part 3—Upper Air and Surface Data Stallion Site.* DR-878, U.S. Army Electronics Command, Jan. 1975. (Available as AD-A007658.)

9. Gridley, Doreen: *Program for Narrow-Band Analysis of Aircraft Flyover Noise Using Ensemble Averaging Techniques.* NASA CR-165867, 1982.

10. Bennett, R. L.; and Pearsons, K. S.: *Handbook of Aircraft Noise Metrics—Final Report.* NASA CR-3406, 1981.

11. Willshire, William L., Jr.; and Garber, Donald P.: En Route Noise Test Preliminary Results. *Proceedings, 1989 International Conference on Noise Control Engineering*, Inter-Noise 89, Volumes 1 & 2, George C. Maling, Jr. ed., Dec. 1989, pp. 309–312.

12. Willshire, William L., Jr.; and Garber, Donald P.: PTA En Route Noise Measurements. *FAA/NASA En Route Noise Symposium*, Clemans A. Powell, comp., NASA CP-3067, 1990, pp. 13–29.

13. Willshire, William L., Jr.; and Garber, Donald P.: Long-Range Verticle Propagation. *Fourth International Symposium on Long-Range Sound Propagation*, William L. Willshire, Jr., comp., NASA CP-3101, 1990, pp. 127–132.

14. Dunn, M. H.; and Tarkenton, G. M.: *Computational Methods in the Prediction of Advanced Subsonic and Supersonic Propeller Induced Noise—ASSPIN Users' Manual.* NASA CR-4434, 1992.

15. Dunn, Mark H.; and Farassat, F.: High-Speed Propeller Noise Prediction—A Multidisciplinary Approach. *AIAA J.*, vol. 30, no. 7, July 1992, pp. 1716–1723.

16. Pierce, Allan D.: *Acoustics—An Introduction to its Physical Principles and Applications.* Acoust. Soc. of America, 1989.

17. American National Standard Method for the Calculation of the Absorption of Sound by the Atmosphere. ANSI S1.26-1978 (ASA 23-1978), American Inst. of Physics, 1978.

18. Bass, H. E.; Sutherland, L. C.; and Zuckerwar, A. J.: Atmospheric Absorption of Sound: Update. *J. Acoust. Soc. America*, vol. 88, no. 4, Oct. 1990, pp. 2019 2021.

19. Sutherland, Louis C.: Review of Experimental Data in Support of a Proposed New Method for Computing Atmospheric Absorption Losses. DOT-TST-75-87, May 1975.

20. Roy, Dipankar: Doppler Frequency Shift for Aircraft Noise in a Refractive Atmosphere. AIAA-84-2354, Oct. 1984.

21. Chien, C. F.; and Soroka, W. W.: Sound Propagation Along an Impedance Plane. *J. Sound & Vib.*, vol. 43, no. 1, Nov. 8, 1975, pp. 9–20.

22. Pao, S. Paul; Wenzel, Alan R.; and Oncley, Paul B.: *Prediction of Ground Effects on Aircraft Noise.* NASA TP-1104, 1978.

23. Bies, David A.: "Acoustical Properties of Porous Materials," *Noise and Vibration Control*, Revised Edition, Leo L. Baranek, ed., Inst. of Noise Control Eng., 1988, pp. 245–269.

REPORT DOCUMENTATION PAGE

Form Approved
OMB No. 0704-0188

1. AGENCY USE ONLY *(Leave blank)*	2. REPORT DATE	3. REPORT TYPE AND DATES COVERED
	September 1994	Technical Paper

4. TITLE AND SUBTITLE
En Route Noise Levels From Propfan Test Assessment Airplane

5. FUNDING NUMBERS
WU 535-03-11-02

6. AUTHOR(S)
Donald P. Garber and William L. Willshire, Jr.

7. PERFORMING ORGANIZATION NAME(S) AND ADDRESS(ES)
NASA Langley Research Center
Hampton, VA 23681-0001

8. PERFORMING ORGANIZATION REPORT NUMBER
L-17339

9. SPONSORING/MONITORING AGENCY NAME(S) AND ADDRESS(ES)
National Aeronautics and Space Administration
Washington, DC 20546-0001

10. SPONSORING/MONITORING AGENCY REPORT NUMBER
NASA TP-3451

11. SUPPLEMENTARY NOTES
Garber: Lockheed Engineering & Sciences Company, Hampton, VA; Willshire: Langley Research Center, Hampton, VA.

12a. DISTRIBUTION/AVAILABILITY STATEMENT
Unclassified–Unlimited

Subject Category 71

12b. DISTRIBUTION CODE

13. ABSTRACT *(Maximum 200 words)*

The en route noise test was designed to characterize propagation of propfan noise from cruise altitudes to the ground. In-flight measurements of propfan source levels and directional patterns were made by a chase plane flying in formation with the propfan test assessment (PTA) airplane. Ground noise measurements were taken during repeated flights over a distributed microphone array. The microphone array on the ground was used to provide ensemble-averaged estimates of mean flyover noise levels, establish confidence limits for those means, and measure propagation-induced noise variability. Even for identical nominal cruise conditions, peak sound levels for individual overflights varied substantially about the average, particularly when overflights were performed on different days. Large day-to-day variations in peak level measurements appeared to be caused by large day-to-day differences in propagation conditions and tended to obscure small variations arising from operating conditions. A three-dimensional ray-tracing method was used to account for atmospheric propagation of sound and predict sound levels on the ground from repeated flights performed at three representative cruise conditions. A parametric evaluation of the sensitivity of this prediction method to weather measurement and source level uncertainties was also performed. In general, predictions showed good agreement with measurements. However, the method was unable to predict short-term variability of ensemble-averaged data within individual overflights. Although variations in absorption appear to be the dominant factor in variations of peak sound levels recorded on the ground, accurate predictions of those levels require that a complete description of operational conditions be taken into account. The comprehensive and integrated methods presented in this paper have adequately predicted ground-measured sound levels. On average, peak sound levels were predicted within 3 dB for each of the three different cruise conditions.

14. SUBJECT TERMS
Ensemble averaging; En route noise; Propfan; PTA; Sound propagation; Sound prediction; Sound measurement

15. NUMBER OF PAGES
31

16. PRICE CODE
A03

17. SECURITY CLASSIFICATION OF REPORT	18. SECURITY CLASSIFICATION OF THIS PAGE	19. SECURITY CLASSIFICATION OF ABSTRACT	20. LIMITATION OF ABSTRACT
Unclassified	Unclassified	Unclassified	

NSN 7540-01-280-5500

Standard Form 298(Rev. 2-89)
Prescribed by ANSI Std. Z39-18
298-102